Monthly Notices
of the
ROYAL ASTRONOMICAL SOCIETY

MNRAS **475,** 5535–5549 (2018) doi:10.1093/mnras/sty010

Dust in the outer layers of the Barnard 5 globule

V. B. Il'in,[1,2,3★] Yu. S. Efimov,[4] T. N. Khudyakova,[1] M. S. Prokopjeva[1★] and V. V. Varivoda[1,5★]

[1] *St Petersburg State University, Universitetskij Pr. 28, St Petersburg 198504, Russia*
[2] *Pulkovo Observatory, Pulkovskoe Sh. 65/1, St Petersburg 196140, Russia*
[3] *St Petersburg University of Aerospace Instrumentation, Bol. Morskaya 67, St Petersburg 190000, Russia*
[4] *Crimea Observatory, Nauchnyj 298409, Crimea*
[5] *Budyonny Military Academy of Telecommunications, Tikhoretsky 3, St. Petersburg 194064, Russia*

Accepted 2017 December 18. Received 2017 December 17; in original form 2017 November 24

ABSTRACT

We present the results of our *UBVRI* polarimetric observations of a dozen stars located close to the well-studied Bok globule Barnard 5 (B5), with several of the stars being seen through its outer layers (with A_V up to ∼3 mag). Using recent astrometric, spectroscopic and photometric surveys, we estimate the distance, spectral class and visual extinction for the observed stars and find that the results are in a good agreement with the available 3D extinction maps. We use a two-layer dust model of interstellar polarization towards B5, in which the layer closer to us is an extension of the Taurus cloud complex, and the farther one (including B5 and its halo) is related to the Perseus cloud complex ($d \approx 280$–350 pc). Using spectral, photometric and polarimetric data on about 30 additional stars, we estimate the parameters of the former layer as $\lambda_{max} \approx 0.56$ μm, $P_{max} \approx 0.7$ per cent, $\theta \approx 50^\circ$, $A_V \approx 0.7$ mag, and show that the observed wavelength dependence of the position angle for the stars observed generally agrees with the two-layer model. We find that when the stars are seen through the globule layers with $A_V = 2$–3 mag, $\lambda_{max} \approx 0.6$–$0.8$ μm, which differs significantly from the $\lambda_{max} = 0.52$–0.58 μm obtained by us for the diffuse interstellar medium in the direction of B5. We discuss the correlation of λ_{max} with the optical thickness into the globule as well as other correlations of the extinction and polarization parameters.

Key words: polarization – ISM: clouds – dust, extinction.

1 INTRODUCTION

Some details of the star-formation process are still unclear; in particular, the physical conditions in small molecular clouds (globules) where low-mass stars are formed are not well understood. Dust is closely related to other components of the interstellar medium (ISM), and therefore the study of its properties in globules could further our understanding.

It is widely believed that the dust grains in dense clouds differ considerably from those located in the diffuse ISM. For instance, Foster et al. (2013) found a correlation between the slope of the extinction law (R_V) and the visual extinction (A_V) at moderate optical depths and interpreted this as evidence for the growth of the grains. Furthermore, scattered light (observed as the core-shine phenomenon, see e.g. Steinacker et al. 2010; Lefèvre et al. 2014) and the submm thermal emission of dust (e.g. Stepnik et al. 2003; Chen et al. 2016) indicate variations in dust properties (including an increase in the mean size of dust grains) with increasing optical depth inside molecular clouds. Larger grains in molecular clouds are manifested by an albedo observed in the range from the *U* to the *I* band (Togi, Witt & St. John 2017). The near-infrared polarization observed for stars behind the cloud IC 5146 suggests a significant growth of the grains in the layers with $A_V > 2.5$ mag (Wang et al. 2017). Grain evolution in molecular clouds is also necessary to explain the polarization observed in the visual and submm ranges (Fanciullo et al. 2017). These and many other observational works have been supplemented with theoretical studies of the evolution of dust in dense clouds (see e.g. Wong, Hirashita & Li 2016; Ysard et al. 2016 and references therein).

The above-mentioned manifestations of the dust evolution do not depend only on the size distribution of the grains. The mean size of particles could be the main parameter, but other parameters may also be significant (see e.g. Fanciullo et al. 2017). Therefore, more observational constraints are required. One of them could be the wavelength at which the interstellar polarization degree reaches its maximum λ_{max}, which could be affected by the mean particle size.

Over the last decade, however, there have been very few new measurements of this parameter for molecular clouds (Fanciullo et al. 2017 considered the visual polarization data of Andersson & Potter 2007, who mostly used earlier observations by other authors).

★ E-mail: ilin55@yandex.ru (VBI); m.prokopieva@spbu.ru (MSP); addams_addams@mail.ru (VVV)

Table 1. List of objects.

Star	Other names	V [mag]	This work	Data in other works
S1	Joshi 18, Cer 110, HD 281155	9.2	*UBVRI*	*GRI* (1), *R* (2)
S2	Per 85, HD 281156	11.1	*UBVRI*	*I* (3)
S3	Joshi 17	13.0	-	*I* (1), *BVRI* (4)
S4	Joshi 16, Per 86	14.0	*VRI*	*RI* (1), *I* (3)
S5	Joshi 1, IRAS 03443+3259	11.7	*BVRI*	*RI* (1), *BVRI* (4)
S6	Joshi 2	13.1	*BVRI*	*GRI* (1)
S7	Cer 116, HD 278995	11.1	*UBVRI*	
S8	Joshi 23, HD 281224	11.2	*UBVRI*	*GRI* (1), *B* (4)
S9	Joshi 24, TYC 2360-688-1	10.7	*BVRI*	*RI* (1), *BVR* (4)
S10	Joshi 11, HD 281217, Per 87	11.0	*UBVRI*	*RI* (1), *I* (3)
S11	Joshi 10	14.3	-	*GRI* (1)
S12	Joshi 6	14.0	*BVRI*	*GRI* (1), *B* (5)

Reference: (i) Joshi NN are the Simbad names for stars observed by Joshi et al. (1985), Per NN means the Simbad name [GBM90] Per NN from Goodman et al. (1990), Cer NNN does [C93] NNN from Černis (1993); (1) Joshi et al. (1985); (2) Andersson & Wannier (1997); (3) Goodman et al. (1990); (4) Il'in et al. (1994); (5) Bhatt (1986).

This is mainly because λ_{max} can be reliably estimated only for stars with a low extinction A_V resulting from a cloud; that is, it cannot provide much-needed information about denser regions. The parameter has been derived previously for many lines of sight through various molecular clouds and the diffuse ISM (see e.g. Voshchinnikov, Il'in & Das 2016). The observational data obtained have demonstrated some correlation of λ_{max} with the optical depth into the clouds (related to the extinction A_V), but for different clouds these dependences are similar and differ by a constant (for more details see Andersson, Lazarian & Vaillancourt 2015).

Because globules differ in some respects from the molecular clouds where λ_{max} has been studied (globules are smaller, more isolated and form only low-mass stars), the study of the parameter λ_{max} in globules is of interest. This parameter can be reliably estimated only for the halo and outer layers of globules (their central parts are too small and opaque), but there are some signs that the properties of dust in these layers should be different from those typical of other globule parts (e.g. Wong et al. 2016; Togi et al. 2017). To date the only study is that by Joshi et al. (1985), who used the data obtained in 2–3 bands by Bhatt (1986) to derive high values of λ_{max} in globule B5 and suggested that these high values could be a result of dust-grain segregation (see also Il'in, Khudyakova & Reshetnikov 1994).

Indeed, globule B5 in the Perseus cloud complex is a good candidate for such a study as it is relatively large (of size 45 arcmin), sufficiently close ($d \sim 300$ pc) and at a high latitude ($l = 161^\circ, b = -17^\circ$): as a result it has been extensively observed and modelled in a variety of ways (e.g. Bally et al. 2008; Zapata et al. 2014; Wirström et al. 2014; Taqu et al. 2017). There is, however, a problem in that the distance of B5 ($d \sim 300$ pc) assumes that there is absorbing material located between the globule and an observer in the form of an extension of the Taurus cloud complex (for details see Bally et al. 2008). The globule possesses an extended neutral halo (see e.g. Bensch 2006) and a patchy core that contains several clumps, protostellar objects and outflows (e.g. Fuller et al. 1991; Pineda et al. 2015). There are, though, enough stars seen through B5 and its halo to perform successful multicolour polarimetric observations.

It is worth noting that the recent *Gaia*, LAMOST and photometric (APASS, TASS, etc.) surveys make polarimetric studies much more informative regarding the properties of dust in the local ISM, as now it is often possible to supplement the polarization data with good estimates of extinction and distance to the stars observed polarimetrically.

In this paper we present the results of our study of the outer layers and vicinity of globule B5 using multicolour polarimetric observations and data available from various sources while taking into account the effects of the dust foreground to B5. In Section 2 we describe our polarimetric observations of several stars seen through B5 and its periphery. In Section 3 we use available astrometric, spectral and photometric data to estimate the distance and extinction to the stars observed. In Section 4 we summarize the information on the distance to B5, on the distribution of dust and on the interstellar polarization in the direction to the part of the Perseus molecular cloud complex containing B5. In Section 5 we describe a two-layer model that is used to analyse the interstellar polarization towards B5 and estimate the parameters of the layer in the foreground of B5. We discuss the results obtained with this model and compare them with earlier studies reported in the literature, with the primary focus being on the correlation between λ_{max} and A_V. We test our model by considering the observational and theoretical wavelength dependences of the position angle. The conclusions are given in Section 6.

2 POLARIMETRIC OBSERVATIONS

Multicolour polarimetric observations of 10 stars in a region of globule B5 were performed with the 2.6-m ZTS and 1.25-m AZT-11 telescopes of the Crimea Astrophysical Observatory in 1990–1992. Table 1 contains a list of our targets supplemented with two additional stars observed by other authors. For all the stars in the table, we give references for available polarimetric data.

Our observations at ZTS were made in the *UBVR* bands in two sets: on 1991 October 4–7 and 1992 October 19–24. We used the standard one-channel polarimeter described by Shakhovskoy & Efimov (1972, 1976); the *UBVR* bands were close to the standard Johnson ones.

The instrumental polarization of the ZTS instrument was estimated from *UBVR* polarimetric observations made by us for four stars: HD 18803 ($V = 6.6$ mag, spectral class G8V, distance 21 pc), HD 42618 (6.8 mag, G4V, 24 pc), HD 154345 (6.7 mag, G8V, 19 pc) and HD 188326 (7.6 mag, G8IV, 56 pc) with zero polarization

according to Appenzeller (1966), Gehrels (1974) and Clayton & Martin (1981).

In order to calibrate the polarization position angle, we made *UBVR* observations of four stars with a high polarization degree: HD 4768 (7.6 mag, B5Ib, ∼1 kpc), HD 25914 (8.1 mag, B6Ia, ∼0.7 kpc), HD 183143 (6.9 mag, B7Iae, ∼2 kpc) and HD 204827 (7.9 mag, B0V, ∼2 kpc). The results obtained and the data from other authors are given in Table 2. Note that the UBG_1O bands used in all three works cited in the table are not the standard Johnson *UBVR* bands (see e.g. Coyne & Gehrels 1967), and therefore a comparison of the results should be done with care. Hereafter, we give the position angle in the equatorial system.

Our observations at AZT-11 were performed in a couple of seasons: 1990 December 14–19; and 1992 November 13–14 and December 26. We used the photometer-polarimeter of Helsinki Univeristy (Piirola 1975; Kerhonen, Piirola & Reiz 1984). Polarization measurements were talen simultaneously in five bands close to the Johnson ones: U ($\lambda_{\rm eff} = 0.36\,\mu$m), B (0.44 μm), V (0.53 μm), R (0.69 μm) and I (0.83 μm). The reduction method and error analysis were standard (see e.g. Huovelin et al. 1989). At least one polarimetric standard star was observed each night. The instrumental polarization redetermined monthly was found to be as small as ∼0.17 per cent and stable (Valtaoja et al. 1991). The mean accuracy of such polarimetric observations was about 0.04 per cent in the U band and about 0.02 per cent in the *BVRI* bands (Jetsu et al. 1990).

The results of our polarimetric observations are presented in Table 3, where the star numbers are as in Table 1. When it was possible to compare our data with those obtained by other authors (such cases can be found in Table 1), we found a reasonable agreement.

Our observational data and the results of other authors are shown in Fig. 1. The effective wavelengths of the bands used in the works cited in Table 1 are as follows. Joshi et al. (1985) and Bhatt (1986) take B ($\lambda_{\rm eff} = 0.445\,\mu$m), G (0.525 μm), R (old) (0.76 μm), I (0.955 μm), all according to Coyne, Gehrels & Serkowski (1974); Andersson & Wannier (1997) take R (0.65 μm); Goodman et al. (1990) take I ($\lambda_{\rm eff} = 0.763\,\mu$m with a passband of about 0.25 μm); Il'in et al. (1994) take AZT14 bands close to the standard Johnson (1966) ones, namely B (0.44 μm), V (0.55 μm), R (0.69 μm), and the AZT-11 bands as given above.

The collected data on the wavelength dependences of polarization were fitted with the Serkowski curve:

$$P(\lambda) = P_{\rm max} \exp[-K \ln^2(\lambda_{\rm max}/\lambda)], \quad (1)$$

where $P_{\rm max}$, $\lambda_{\rm max}$ and K are the parameters. For most stars, we did not have good enough data to estimate all three parameters and used the relationship $K = 1.7\,\lambda_{\rm max}$ (Whittet et al. 1992).

Our fitting was made using the Levenberg–Marquardt method (Press et al. 2007), and the results are presented in Table 4, where we also show χ^2 normalized by the degrees of freedom to characterize the fits.

Note that Bhatt (1986) used the polarimetric data obtained in 2–3 bands to estimate the values of $P_{\rm max}$ and $\lambda_{\rm max}$ for several stars in the vicinity of B5. Considering his results, we see that our observations supplemented with the data obtained by other authors reduce the uncertainties of $\lambda_{\rm max}$ in 2–4 times (bringing them mostly to the level of 0.02–0.04 μm) and significantly correct the values of $\lambda_{\rm max}$ for some reddened stars (in particular, S5, S6, S8, S11, S12). This improvement made a deeper analysis of the polarimetric data possible.

Note also that for several stars we detected small systematic changes of the position angle with the wavelength. These variations are discussed in Section 5.2.4.

3 DISTANCE AND EXTINCTION TO THE STARS OBSERVED

We use various astrometric, photometric and spectroscopic surveys to estimate the distance and extinction to the stars in Table 1.

The spectral types of the stars were compiled from spectral (HDE, Nesterov et al. 1995; LAMOST DR2, Luo et al. 2016) data or Vilnius photometry (Černis 1993), and when such data were not available from *JHK* (2MASS, Skrutskie et al. 2006) data following the approach of Maheswar et al. (2010). In the latter case, we used the intrinsic colours $(J-H)_0$, $(H-K_s)_0$ from Straižys & Lazauskaite (2009), and $E(J-H)/E(H-K_s) = 1.77$ and $E(H-K_s) = 0.061A_V$ according to the mean Galactic extinction curve from Cardelli, Clayton & Mathis (1989). There are different estimates of the ratio varying from 1.9–2.0 to 1.6 (see e.g. Naoi et al. 2006; Wang & Jiang 2014; Damineli et al. 2016), but this does not have much of an effect on our estimates. The relationship between $T_{\rm eff}$, $\log g$ and the spectral type was taken from Straižys (1992).

The distance d was calculated from the *Gaia* DR1 parallax (Gaia collaboration 2016), when available, and otherwise from the relationship $X = M_V - (V-X)_0 + 5\log d/10$, where $X = V$ or K when V was unknown, while the intrinsic colour $(V-K)_0$ and the absolute stellar magnitude in visual M_V were taken from Straižys (1992).

The visual extinction was estimated using the relationship (e.g. Voshchinnikov & Il'in 1987) $A_V = 1.1E(V-K_s) = 1.1[(V-K_s) - (V-K_s)_0]$, where $(V-K_s)_0$ was from Straižys & Lazauskaite (2009). The constant in the relationship is known to depend weakly on the parameters (Whittet et al. 2008), and the accuracy of A_V is limited by the classification errors rather than by the uncertainty of the intrinsic colour. The colour excess $E(B-V)$ and the ratio $R_V = A_V/E(B-V)$ were not considered by us, because for our stars the data available in the B band are mostly unreliable.

The photometric data in the V band were compiled from APASS DR9 (Henden et al. 2016), Tycho 2 (Hog et al. 2000) and TASS Mark IV (Droege, Richmond & Sallman 2006), and those in the J, H, K_s bands from 2MASS.

Other observational data were also used if available. We consider all the stars in some detail in Appendix A and present our estimates of visual extinction and distance in Table 4. Note that for some stars the available data are controversial, and the uncertainties of d and A_V could not be evaluated accurately.

The described approach can be called the intrinsic colour method, in contrast to the more accurate method based on fitting the spectral energy distribution (see e.g. McDonald, Zijlstra & Watson 2017). Our use of the simplified approach is motivated by the low accuracy of the photometric data in the B and V bands (2MASS J, H, K data are not sufficient for accurate stellar classification) and by the desire to include as much available data as possible.

4 INTERSTELLAR EXTINCTION AND POLARIZATION IN THE DIRECTION OF B5

It is important to note that it is not only the dust in the globule that contributes to the extinction and polarization measured for our stars. In order to estimate the contribution of the globule, it is necessary to consider the distribution of the absorbing material along the lines of sight towards B5, to estimate the distance to the globule, and to analyse the interstellar polarization distribution.

In Appendix B we consider the information on the interstellar extinction in the area of B5 provided by recent extinction surveys, as

Table 2. Observations of standard stars.

Star	P_U [per cent]	θ_U [°]	P_B [per cent]	θ_B [°]	P_V [per cent]	θ_V [°]	P_R [per cent]	θ_R [°]	Data source
HD 4768	2.07 ± 0.04	81.0	2.15 ± 0.04	80.7	2.11 ± 0.04	80.3	1.94 ± 0.04	81.3	Z91
HD 4768	2.30 ± 0.05	81.2	2.36 ± 0.03	81.7	2.37 ± 0.03	82.7	2.37 ± 0.08	79.1	(1)
HD 4768	2.15 ± 0.04	79.9	2.39 ± 0.02	80.6	2.50 ± 0.08	81.5	2.33 ± 0.09	82.9	(1)
HD 25914	4.15 ± 0.07	141.3	4.72 ± 0.06	141.4	4.85 ± 0.05	141.2	4.30 ± 0.07	138.8	Z91
HD 25914	4.08 ± 0.06	139.4	4.56 ± 0.02	141.2	4.65 ± 0.03	141.2	4.34 ± 0.08	139.5	(1)
HD 25914	4.08 ± 0.07	140.5	4.27 ± 0.03	139.3	4.58 ± 0.04	139.9	4.45 ± 0.09	137.4	(1)
HD 183143	4.59 ± 0.05	179.1	5.28 ± 0.03	178.4	5.81 ± 0.04	179.0	5.25 ± 0.03	179.4	Z92
HD 183143	4.92 ± 0.06	180.1	5.89 ± 0.08	178.7	6.09 ± 0.08	179.5	5.82 ± 0.03	177.8	(2)
HD 183143	4.79 ± 0.05	178.7	5.65 ± 0.01	178.8	6.05 ± 0.02	179.2	5.73 ± 0.06	179.0	(2)
HD 204827	5.45 ± 0.08	57.0	5.67 ± 0.05	58.5	5.37 ± 0.03	59.0	4.46 ± 0.04	58.9	Z91
HD 204827	5.64 ± 0.05	59.1	5.78 ± 0.03	60.4	5.59 ± 0.04	60.2	4.59 ± 0.05	60.5	Z92
HD 204827	5.49 ± 0.20	59.4	5.56 ± 0.10	60.6	5.50 ± 0.10	60.4	4.79 ± 0.10	62.0	(3)

References: Z91 denotes this work (1991 set); Z92, this work (1992 set); (1) Coyne & Gehrels (1967); (2) Coyne & Wickramasinghe (1969); (3) Serkowski, Gehrels & Wisniewski (1969).

Table 3. Results of polarimetric observations.

Star	P_U [per cent]	θ_U [°]	P_B [per cent]	θ_B [°]	P_V [per cent]	θ_V [°]	P_R [per cent])	θ_R [°]	P_I [per cent]	θ_I [°]	Obs. set
S1	0.60 ± 0.06	31.9	0.69 ± 0.46	26.2	0.88 ± 0.07	30.0	0.61 ± 0.05	31.2	0.56 ± 0.05	22.9	A92
S2	1.04 ± 0.14	13.7	1.25 ± 0.05	7.7	1.27 ± 0.09	3.8	1.22 ± 0.05	3.0	1.12 ± 0.05	3.7	A92
S4					1.67 ± 1.14	153.1	1.90 ± 0.14	141.2	2.13 ± 0.19	139.5	A92
S5			1.74 ± 0.27	2.6	2.12 ± 0.09	2.8	2.10 ± 0.11	4.8			Z91
S5			3.12 ± 0.60	172.5	1.88 ± 0.23	5.7	1.95 ± 0.08	5.1	1.90 ± 0.06	2.4	A92
S5			1.24 ± 0.19	6.2	1.97 ± 0.09	7.6	1.87 ± 0.10	5.5			Z92
S6			1.53 ± 0.23	54.7	1.50 ± 0.20	45.3	2.25 ± 0.05	43.0	2.14 ± 0.06	43.8	A92
S6			1.75 ± 0.18	45.9	1.93 ± 0.10	46.2	2.43 ± 0.14	40.6			Z92
S7	0.94 ± 0.15	33.0	1.03 ± 0.05	39.0	1.14 ± 0.12	38.0	0.99 ± 0.07	40.0	0.85 ± 0.10	34.0	A90
S8	0.99 ± 1.07	2.8	2.19 ± 0.10	14.5	2.13 ± 0.07	12.1	2.01 ± 0.15	7.6			Z91
S8	1.08 ± 0.43	20.0	2.07 ± 0.14	11.2	1.92 ± 0.16	10.7	1.90 ± 0.06	9.0	1.52 ± 0.08	6.2	A92
S9			0.67 ± 0.34	17.7	1.30 ± 0.18	16.8	0.96 ± 0.09	14.6			Z91
S9			0.61 ± 0.18	10.9	0.98 ± 0.08	12.1					Z91
S9			1.26 ± 0.55	29.0	1.69 ± 0.12	18.9	0.88 ± 0.07	27.4	0.94 ± 0.04	22.4	A92
S10	0.59 ± 0.16	65.0	0.69 ± 0.09	59.7	0.62 ± 0.12	62.1	0.71 ± 0.03	51.8	0.68 ± 0.07	62.1	A92
S12			3.63 ± 0.44	34.2	3.04 ± 0.58	27.6	3.67 ± 0.26	40.1	3.06 ± 0.18	44.5	A92

Notes: A90 refers to observations from the AZT-11 in 1990; A92 to AZT-11 in 1992; Z91 to ZTS in 1991; and Z92 to ZTS in 1992.

Table 4. Polarization and other parameters of the stars.

Star	$P_{\max}$ [per cent]	$\langle\theta\rangle$ [°]	$\lambda_{\max}$ [μm]	χ^2/df	A_V [mag]	d [pc]	Sp. type	Sources
S1	0.717 ± 0.014	30	0.577 ± 0.025	2.0	0.9 ± 0.3	125 ± 20	F0 V	Vi,HD
S2	1.301 ± 0.028	5	0.560 ± 0.025	0.6	1.0 ± 0.2	200 ± 20	F5 V	Ga,La,HD
S3	1.729 ± 0.111	160	0.654 ± 0.084	4.4	3.2 ± 0.5	660 ± 200	K2 III	JHK
S4	2.145 ± 0.188	140	0.920 ± 0.116	0.3	2.8 ± 0.2	1450 ± 200	K3.5 III	La
S5	2.098 ± 0.023	5	0.733 ± 0.016	3.6	3.7 ± 0.5	315 ± 150	K1 III	JHK
S6	2.250 ± 0.034	45	0.762 ± 0.023	1.6	3.1 ± 0.2	690 ± 100	G9.5 III	La
S7	1.063 ± 0.037	35	0.519 ± 0.045	0.2	0.5 ± 0.1	270 ± 25	F4 V	Ga,Vi,La,HD
S8	2.066 ± 0.036	10	0.536 ± 0.022	3.1	1.6 ± 0.1	540 ± 95	F4.5 III	Ga,La,HD
S9	1.049 ± 0.034	15	0.581 ± 0.037	2.8	2.4 ± 1.2	800 ± 200	M4 III	JHK,Sp
S10	0.721 ± 0.031	60	0.584 ± 0.057	0.6	0.6 ± 0.3	330 ± 45	F9 IV	Ga,La,HD
S11	3.973 ± 0.737	5	0.574 ± 0.199		2.8 ± 0.5	600 ± 400	G5 IV	La
S12	3.691 ± 0.091	35	0.648 ± 0.034	1.9	2.3 ± 0.2	380 ± 90	F5.5 V	La

Notes: The sources of parallax and spectral data are as follows: Ga stands for *Gaia* DR1 data (Gaia collaboration 2016); La for LAMOST DR2 data (Luo et al. 2016); Vi for the Vilnius photometry of Černis (1993); HD for HDE data from Nesterov et al. (1995); JHK for 2MASS photometry (Skrutskie et al. 2006); and Sp for other spectral data (see text).

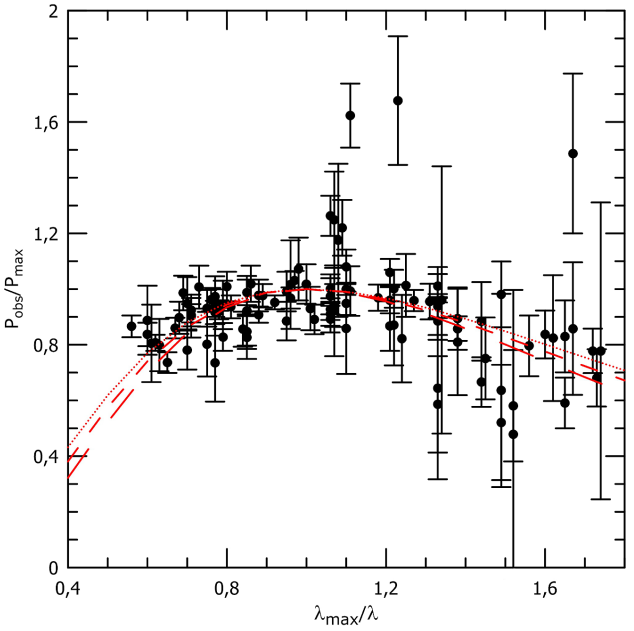

Figure 1. The wavelength dependence of the observed polarization degree P_{obs} normalized using the obtained values of P_{max} and λ_{max} (see the text and Table 4). The data derived by us and other authors are presented for all stars in Table 1. The Serkowski curve (1) is shown for $K = 1$ (dotted line), 1.2 (dashed line), 1.5 (long-dashed line) to illustrate the effect of the parameter changes (in this work, $K = 1.7\lambda_{max}$ is used).

well as by some studies of the Perseus complex. This consideration allows us to draw the following conclusions.

There are two layers of absorbing material towards B5 and its surrounding regions: one is located at the distance $d \approx 130$–160 pc (perhaps extending up to about 200 pc) and another at $d \sim 260$–350 pc. The first (closest to the observer) layer related to the Taurus complex is more or less homogeneous on large scales, with $A_V \approx 0.8 - 0.9$ mag; the second one is patchy. The latter includes globule B5 with its extended halo and many other clouds but it is not observed towards the central parts of the Per OB2 association (the regions to the north and east of B5). There appears to be no significant extinction beyond $d > 500$ pc, and the contribution of the H I supershell around the association (Bally et al. 2008) seems to be small.

If globule B5 is physically associated with the IC 348 clouds, then the distance to it should be $d(\mathrm{B5}) = 300 \pm 15$ pc. However, if the results of Schlafly et al. (2014) are correct, then d(B5) is slightly larger ($\sim$350 pc).

In order to analyse the interstellar polarization towards B5, we collected stars with measured polarization located within $\sim$1°.5 of the globule. As we are interested mainly in interstellar polarization (i.e. polarization not formed in dense clouds), only stars with $A_V \lesssim 2$ mag were considered. In total, we found 35 such stars: 6 stars (S1–2, S7–10) have already been presented in Table 4, and the 29 additional stars are given in Table 5.

Table 5 provides the coordinates, the distance derived nearly for all stars from the *Gaia* parallax, the spectral class found in the literature, the extinction A_V estimated as described in Section 3, and the polarization data with their reference. Note that our estimates agree within the uncertainties with the values obtained for several stars by other authors (Neckel et al. 1980; Černis 1993; Wegner 2003).

The general behaviour of the interstellar polarization vectors is shown in Fig. 2. Its main features are as follows.

(i) The region N located to the north of B5 ($\delta > 33°40'$) includes the stars A1, A3, A24, A26 from Table 5. They have a similar position angle $\theta = 88° \pm 12°$, a polarization degree $P = 0.7 \pm 0.2$ per cent and $A_V = 0.8 - 1.0$ mag, which is in good agreement with the mean value $\langle A_V \rangle = 0.95$ mag expected for the OB2 association members located in this region (Černis 1993). The distance to the stars is $d = 260$–400 pc, and so, indeed, we do not have significant extinction in the second layer and the interstellar polarization observed is related to the first layer.

(ii) The region E located to the east of B5 ($\alpha > 3^{h}49^{m}$, $\delta < 33°20'$) includes the stars A15–16, A19–20, A22–23 and A27–28. They also have a similar (but different) position angle, $\theta = 53° \pm 10°$, the polarization degree is on average higher, $P = 0.9 \pm 0.2$ per cent, but $A_V = 0.6 - 1.2$ mag is still in agreement with the mean $\langle A_V \rangle = 0.95$ mag from Černis (1993).

In both these regions the extinction is low; that is, we observe just the first layer related to the Taurus complex. The direction of the polarization vectors agrees well with that measured for the region with *Planck* (Planck collaboration XIX 2015): $\theta_{submm}(\mathrm{N}) \approx 85°$ and $\theta_{submm}(\mathrm{E}) \approx 60°$. The dispersion of the submm polarization vectors in the regions N and E is low-to-medium, which also agrees with our results in the visual bands.

Thus, we conclude that the parameters of the interstellar polarization caused by dust in the first layer vary weakly in the field shown in Fig. 3. Note, however, the systematic difference of the position angle by $\Delta\theta \approx 30°$ between the N and E regions. This difference, also observed by *Planck*, probably reflects large-scale variations of the magnetic field in the Taurus–Perseus–Auriga complex.

(iii) The south-western (corner) region SW ($\alpha < 3^{h}46^{m}$, $\delta < 32°30'$) is part of the IC 348 cloud, being a place of active star formation. However, the position angle of the stars A4–7 and A10 varies weakly ($\theta = 34° \pm 11°$), as well as the degree $P = 1.0 \pm 0.5$ per cent and $A_V = 1.0 \pm 0.3$ mag; in particular, for the well-known star o Per (A4) located at $d = 340^{+120}_{-70}$ pc, we have $A_V \approx 0.9$ mag, $P_V \approx 0.6$ per cent and $\theta = 23°$. Probably, for this and four other stars the observed extinction and polarization originate mainly in the first layer.

The interstellar polarization towards the IC 348 cloud and the Perseus complex was studied by Goodman et al. (1990). They found a random distribution of about 40 per cent of the polarization vectors for the complex and a bimodal distribution of other vectors: smaller-polarization-degree vectors have $\theta = 71° \pm 12°$, while larger-degree ones have $\theta = 145° \pm 8°$. A similar bimodal distribution was found in earlier studies, but the distribution parameters were different (see Vrba, Ström & Ström 1976; Turnshek, Turnshek & Craine 1980; Joshi et al. 1985). Keeping in mind that Goodman et al. (1990) were not concentrating on the IC 348 cloud and in particular on its northern part, we suggest that our stars better reproduce the polarization behaviour, namely that in the SW region the polarization formed mostly in the first layer is fairly regular and tilted by $\theta \approx 20°$ relative to the polarization in the E region.

There is, however, a strange group of four stars, namely A13, S2, S8–9, located close to the southern border of B5 (hereafter region S). The position angle for these stars is $\theta = 2° \pm 8°$ ($P = 1.5 \pm 0.5$ per cent, $A_V = 1.3 \pm 0.3$ mag). It differs by about 30° from the angle for several surrounding stars (A8, A10, A15 and S1), which is equal to $\theta = 36° \pm 6°$ ($P = 1 \pm 0.4$ per cent, $A_V = 0.7 \pm 0.1$ mag). The reason for this difference is not clear. It could be related to a contribution from the second layer, as the stars in region S show a greater extinction (by $\sim$0.6 mag) and higher polarization degree

Table 5. Additional stars with measured polarization ($A_V \lesssim 2$ mag) in the vicinity of B5.

Star	Name	α, δ (2000)	d [pc]	Sp	$A_V^{(c)}$ [mag]	P [per cent]	θ [°]	Band	Ref.
A1	HD 22951	03 42 22.65+33 57 54.1	320^{+23}_{-21}	B1V	0.8 ± 0.1	0.8 ± 0.03	76 ± 1	R	(5)
A2	HD 278934	03 43 14.92+33 35 16.0	310^{+30}_{-25}	A0V	1.6 ± 0.3	1.5 ± 0.11	49 ± 3	R	(5)
A3	HD 23060	03 43 24.01+34 06 58.5	390^{+55}_{-43}	B2Vp	1.0 ± 0.1	0.5 ± 0.2	82 ± 8	$V^{(d)}$	(1)
A4	HD 23180	03 44 19.13+32 17 17.7	$340^{+120\,(a)}_{-70}$	B1III	0.9 ± 0.2	0.6 ± 0.2	23 ± 8	$V^{(d)}$	(1)
A5	[GPM90] Per 74	03 44 23.77+32 29 23.6	$320 \pm 80^{(a)}$	G4V	1.7 ± 0.2	0.79 ± 0.16	27 ± 6	$R^{(d)}$	(3)
A6	HD 23322	03 45 27.06+32 17 15.5	200^{+14}_{-13}	K0III	0.8 ± 0.2	0.63 ± 0.06	39 ± 3	$R^{(d)}$	(3)
A7	[C93] 104	03 45 56.68+32 12 43.3	240^{+18}_{-15}	G2V	0.7 ± 0.2	0.40 ± 0.09	53 ± 7	$R^{(d)}$	(3)
A8	TYC 2360-397-1	03 46 09.65+32 46 41.1	250^{+38}_{-30}	F8V$^{(b)}$	0.7 ± 0.3	0.58 ± 0.09	43 ± 5	$R^{(d)}$	(3)
A9	TYC 2360-20-1	03 46 35.46+32 51 48.8	120 ± 4	G8.5V	0.4 ± 0.2	0.11 ± 0.11	–	I	(2)
A10	HD 23478	03 46 40.87+32 17 24.7	290^{+48}_{-36}	B3IVe	0.9 ± 0.1	1.45 ± 0.03	28 ± 1	I	(4)
A11	HD 278994	03 47 27.77+33 19 29.6	580^{+124}_{-87}	A0III	1.1 ± 0.2	0.79 ± 0.16	24 ± 6	V	(4)
A12	HD 23625	03 47 52.67+33 35 59.5	360^{83}_{57}	B2.5V	0.9 ± 0.2	0.52 ± 0.06	17 ± 3	V	(4)
A13	HD 281226	03 48 29.49+32 18 18.5	$360 \pm 80^{(a)}$	A1V	1.5 ± 0.2	1.0 ± 0.11	174 ± 3	V	(6)
A14	TYC 2360-7-1	03 49 00.23+33 06 38.9	190^{+9}_{-8}	G4V	0.7 ± 0.1	0.36 ± 0.13	78 ± 10	I	(2)
A15	HD 23802	03 49 07.32+32 15 51.6	260^{+31}_{-25}	B5Vn	1.0 ± 0.1	1.07 ± 0.07	42 ± 2	V	(4)
A16	HD 281218	03 49 09.16+32 48 47.1	250^{+46}_{-35}	F7.5V	0.6 ± 0.2	0.59 ± 0.10	57 ± 5	$R^{(d)}$	(3)
A17	HD 279065	03 49 24.09+32 58 18.4	1300^{+3700}_{-600}	K5III	1.7 ± 0.5	0.71 ± 0.02	57 ± 1	V	(2)
A18	HD 23848	03 49 32.69+33 05 29.0	$90^{+7\,(a)}_{-6}$	A3V	0.1 ± 0.1	0.03 ± 0.12	–	$B^{(d)}$	(1)
A19	HD 279064	03 49 56.46+33 06 09.7	450^{+55}_{-43}	F0	1.2 ± 0.3	1.4 ± 0.08	43 ± 2	V	(6)
A20	HD 281223	03 50 25.62+32 26 17.0	460^{+86}_{-63}	A0	0.9 ± 0.3	0.7 ± 0.07	68 ± 3	V	(6)
A21	HD 23974	03 50 27.51+31 33 13.0	300^{+28}_{-24}	B8V	1.0 ± 0.3	1.8 ± 0.04	64 ± 1	R	(5)
A22	HD 24039	03 50 58.87+32 10 10.5	190^{+11}_{-10}	A3IV	1.1 ± 0.2	1.0 ± 0.05	48 ± 1	V	(6)
A23	HD 24038	03 51 01.45+32 33 30.2	160^{+53}_{-32}	A7V	0.8 ± 0.3	0.7 ± 0.03	28 ± 1	V	(6)
A24	HD 24131	03 51 53.72+34 21 32.8	260^{+27}_{-22}	B1V	0.8 ± 0.1	0.9 ± 0.03	94 ± 1	R	(5)
A25	HD 279128	03 52 16.28+33 24 22.2	1300^{+700}_{-340}	A0II	2.2 ± 0.3	1.2 ± 0.05	85 ± 1	R	(5)
A26	HD 24190	03 52 18.96+34 13 19.6	400^{+61}_{-46}	B2V	0.9 ± 0.1	0.5 ± 0.2	100 ± 8	$V^{(d)}$	(1)
A27	HD 279137	03 52 22.93+32 53 44.1	770^{+270}_{-160}	A1V	0.4 ± 0.2	1.1 ± 0.12	58 ± 3	V	(6)
A28	HD 279133	03 52 36.96+33 07 36.0	560^{+115}_{-80}	A1V	0.6 ± 0.2	1.0 ± 0.09	71 ± 3	V	(6)
A29	HD 24398	03 54 07.92+31 53 01.1	230^{+11}_{-9}	B1Ib	1.0 ± 0.1	1.13 ± 0.03	62 ± 1	$B^{(d)}$	(1)

Notes: (a) the distance is derived not from the *Gaia* parallax but as described in Section 3; (b) the spectral class, not found in the literature, was estimated as described in Section 3; (c) A_V is derived as suggested in Section 3; (d) not the standard band. References to the polarization data are as follows: (1) early observations catalogued by Heiles (2000); (2) Joshi et al. (1985); (3) Goodman et al. (1990); (4) Il'in et al. (1994); (5) Andersson & Wannier (1997); (6) Efimov (1997, private communication).

(by 0.5 per cent), being mostly located at $d > 350$ pc, while all four surrounding stars have $d = 125$–290 pc. However, the star S2 is certainly at $d = 200$ pc according to its *Gaia* parallax. Thus, when considering the interstellar polarization of stars seen through the southern part of B5 and its halo, one must keep in mind the noted effect of unclear nature. Generally, the distribution of the stellar polarization vectors in the B5 field is typical of that observed for other dark clouds (see e.g. Sen et al. 2005).

5 DISCUSSION

To start with, we compare our results with the extinction map of the B5 region obtained within the COMPLETE project (Ridge et al. 2006). The comparison made in Fig. 3 reveals a good correlation of our estimates of the extinction A_V to the observed stars with the mapped extinction, and a reasonable correlation between this extinction and the wavelength of maximum polarization λ_{max}.

In particular, it can be seen that the stars in the background of B5 (S3–6, S11–12) according to their distance (also S5, if $d(\mathrm{B5}) < 315 \pm 150$ pc) have an extinction A_V of about 3 mag, in good agreement with the map. The remaining stars (S1–2, S7–10) are either foreground according to their distance (S1–S2, S7, and S10 if $d(\mathrm{B5}) > 330 \pm 45$ pc) or are distant from B5 (S8, S9). The foreground stars have low extinction, $A_V = 0.6 - 1$ mag, and for the more distant stars S9, S10, $A_V \gtrsim 1.5$ mag. It should be noted that the agreement of our results with the map becomes even better if we take into account that the lines of equal A_V values in Fig. 3 are too smoothed as seen from a more detailed extinction map of Foster et al. (2013).

More important, however, is the relationship between λ_{max} values and the position of the stars. The figure shows that for stars background to B5 ($A_V \sim 3$ mag, i.e. the contribution of B5 to extinction is

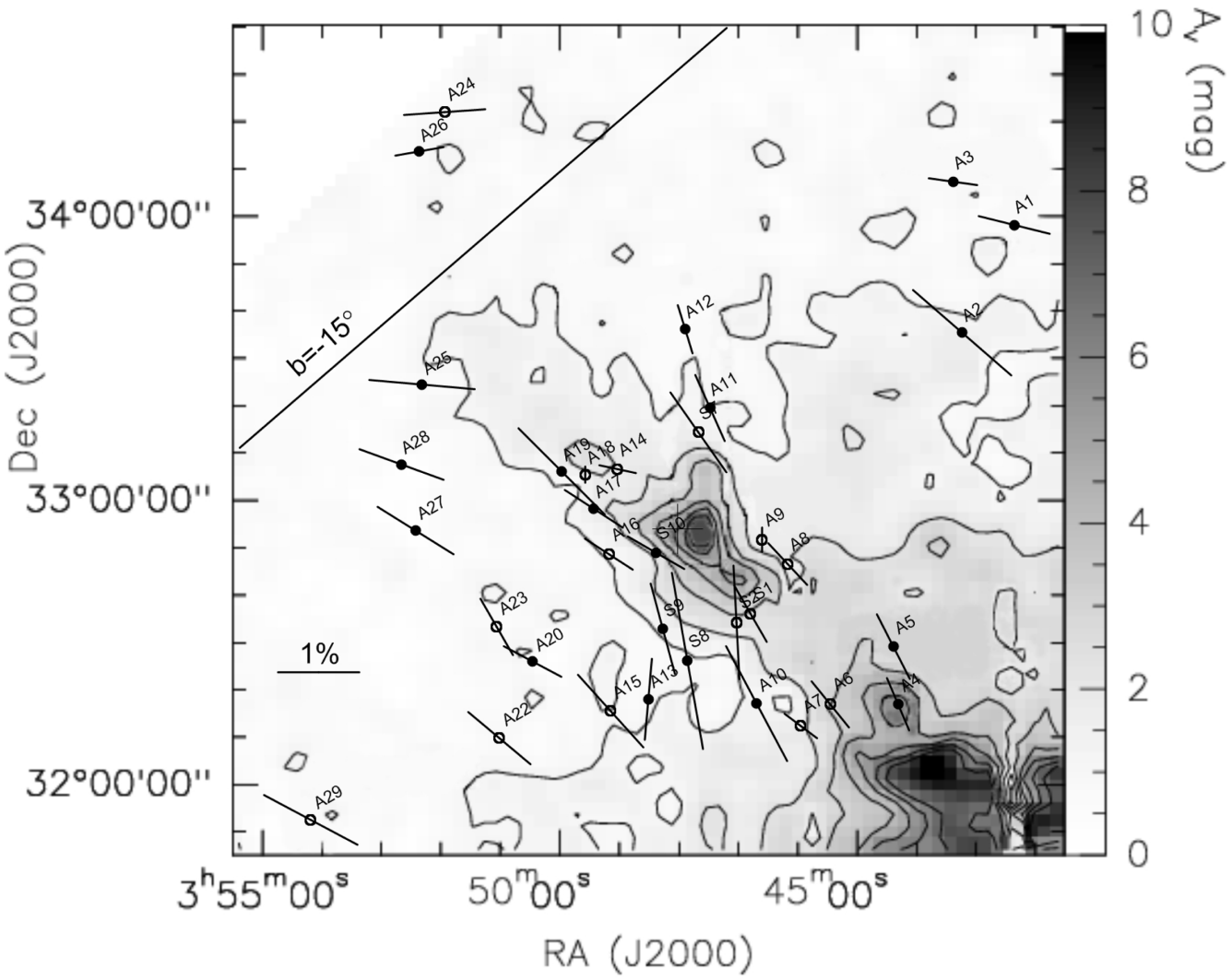

Figure 2. Interstellar polarization in the vicinity of globule B5. The vectors show the direction of linear polarization for stars from Tables 4 and 5; the length of the vectors is proportional to the polarization degree. Open circles refer to stars that are certainly in the foreground of B5 ($d < 270$ pc). The COMPLETE extinction map of the B5 region is from (Bensch 2006). The line labelled $b = -15^\circ$ is parallel to the Galactic plane.

significant) we derive $\lambda_{max} \approx 0.7$–$0.9$ μm. For the foreground stars and stars away from B5, we have with good accuracy (∼0.035 μm) values of $\lambda_{max} = 0.52 - 0.58$μm, which are typical of the diffuse ISM. This relationship needs a more accurate consideration, as given below.

5.1 Dust foreground to B5

Using the knowledge on the interstellar extinction and polarization gained in Section 4, we can consider the results of our observations in more detail. The stars foreground to or located away from B5 according to Table 4 and the stars from Table 5 can be used to define the parameters of interstellar polarization caused by dust in the Taurus complex (hereafter the first layer of dust). Then by subtracting the contribution of this layer we can estimate the parameters of extinction and polarization produced by dust in the globule from the data for the stars background to B5.

In Tables 4–5, there are 14 stars at a distance $100 < d < 260$ pc, that is, certainly located foreground to B5 and the nearby part of the Perseus complex. For these stars, we obtain the mean value $\langle A_V \rangle = 0.8 \pm 0.2$ mag, in very good agreement with the estimate in Appendix B ($A_V = 0.7$–0.95 mag). The stars are distributed in a region of radius of about 1.°4. When considering a smaller region (a radius of about 0.°4) centred at B5, we find seven stars (S1, S2, S7, S10, A8, A14, A16) and a slightly smaller value of $\langle A_V \rangle = 0.7 \pm 0.2$ mag. The stars observed and seen through B5 are separated by less than 30 arcmin (1.4 pc at $d = 160$ pc), and we assume that they have the same extinction, which is the first parameter of the dust layer in the foreground of B5.

For four stars (S1, S2, S7, S10) in the 0.°4 radius region, we have estimates of the wavelength of maximum polarization varying from 0.52 to 0.58 μm with a mean value of $\langle \lambda_{max} \rangle = 0.56 \pm 0.03$ μm, which is typical of the diffuse ISM. The stars S8, S9, which do not project on B5, are slightly more reddened, but still have $\lambda_{max} = 0.54$ and 0.58 μm.

Estimates of the maximum polarization degree in the foreground layer are less reliable. From seven stars within the 0.°4 region, we excluded one (S2) as it is in the strange region S (see the end of Section 4). For stars A8, A14 and A16, the polarization was observed in the *R* and *I* bands, but using the Serkowski law with $\lambda_{max} = 0.56$ μm

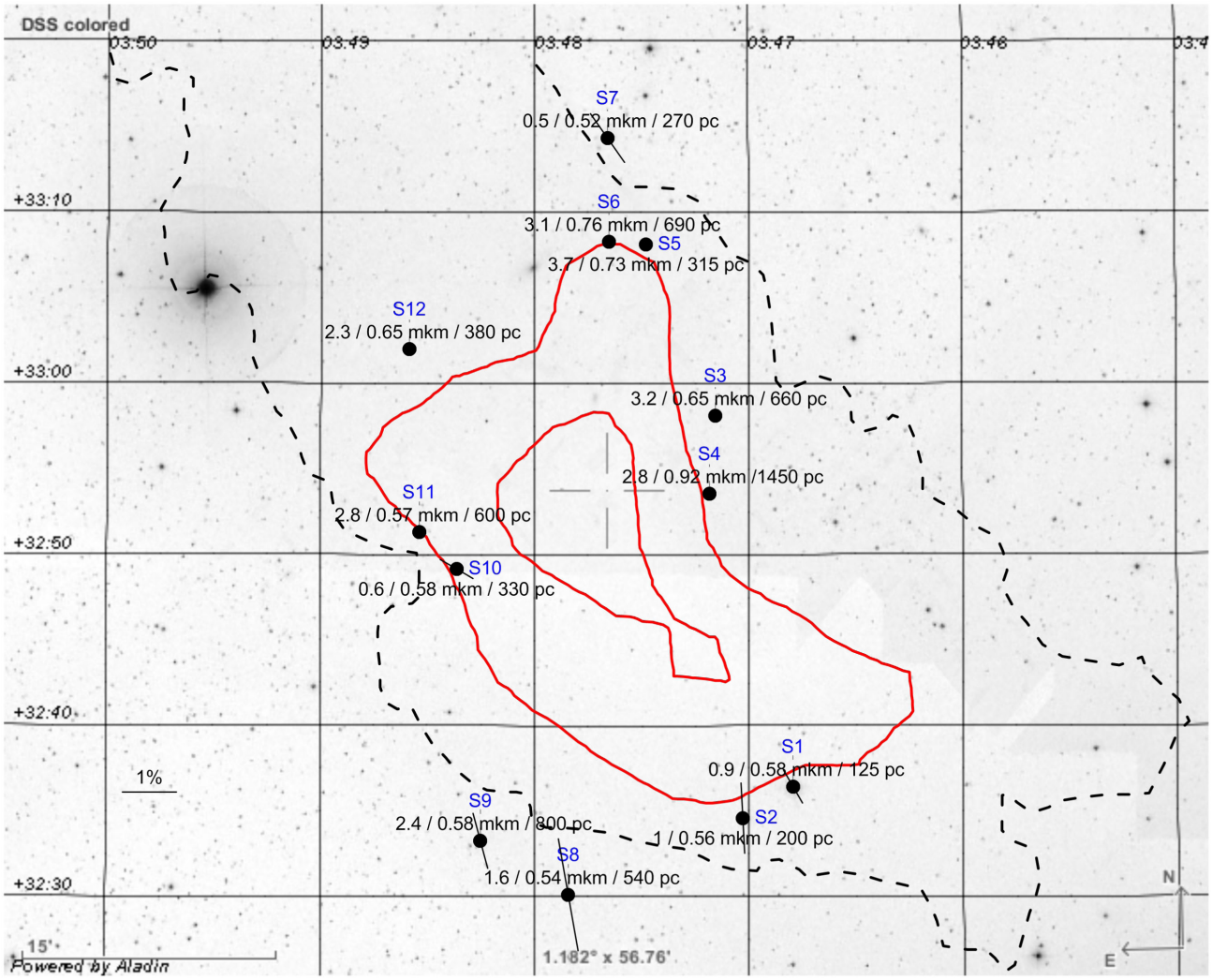

Figure 3. Position of the stars from Table 1 on a stellar map. The cross indicates the centre of the B5 image. The solid (red) lines show the contour lines of extinction $A_V = 3$ and 5 mag, and the dashed line illustrates the ^{13}CO(1 − 0) integrated intensity distribution according to the COMPLETE results (Ridge et al. 2006). Numbers at the stars give the obtained values of A_V, λ_{max}, and distance d (see Table 4), and the vectors show the stellar polarization.

(see above) we can estimate P_{max}. So, for the remaining six stars in the 0.°4 region, we derive P_{max} in the range 0.5–1.1 per cent with the mean value $\langle P_{max}\rangle = 0.75 \pm 0.25$ per cent.

With the assumption that the magnetic field in the foreground layer does not change significantly at the distance of 1.4 pc in the sky plane, we obtain the following estimates of the position angle θ. Using the six stars (S1, S7, S10, A8, A14, A16) mentioned in the previous paragraph, we obtain a mean position angle in the visual of $\langle\theta_V\rangle = 50^\circ \pm 20^\circ$. This value coincides with the mean position angle in region E (see Section 4). Note the systematic change of the position angle (the orientation of the magnetic field in the foreground layer) from region N ($\theta \approx 90^\circ$) to region E and B5 ($\theta \approx 50^\circ$) to region SW ($\theta \approx 35^\circ$).

5.2 Dust in globule B5

5.2.1 *Correction for the foreground material*

We apply the following two-layer model of polarization formation in the direction of B5. The first (nearest to the observer) dust layer causes polarization $P_1(\lambda)$, described by the Serkowski law (1) with the parameters $P_{max,1}$ and $\lambda_{max,1}$. The layer is homogeneous and uniform; that is, for all stars seen through it alone, the extinction $A_{V,1}$, the polarization degree $P(\lambda)$ and the position angle $\theta(\lambda) \equiv \theta_1$ are constant. Based on the considerations above, we adopt $A_{V,1} = 0.7 \pm 0.2$ mag, $P_{max,1} = 0.75 \pm 0.25$ per cent, $\lambda_{max,1} = 0.56 \pm 0.03$ μm and $\theta_1 = 50^\circ \pm 20^\circ$. The second layer is inhomogeneous; that is, the extinction $A_{V,2}$ and the polarization parameters $P_{max,2}, \theta_{V,2}$ vary from one line of sight to another. Because this layer is associated with the globule, we assume that $A_{V,2}$ and $P_{max,2}$ are significantly larger than $A_{V,1}$ and $P_{max,1}$, respectively.

If a star is seen through both layers, the observed extinction and linear polarization are (see e.g. Martin 1978):

$$A_V^{obs} = A_{V,1} + A_{V,2}, \quad \boldsymbol{P}^{obs}(\lambda) = \boldsymbol{P}_1(\lambda) + \boldsymbol{P}_2(\lambda), \tag{2}$$

where the polarization vector $\boldsymbol{P}$ has length equal to the polarization degree P and direction defined by the double position angle θ; that is, the components of $\boldsymbol{P}$ are as usual $P_x = P\cos 2\theta$, $P_y = P\sin 2\theta$, being the normalized Stokes parameters.

Using equations (2), we can derive the parameters of the second layer if we know the polarization observed for a star seen through both layers ($P^{obs}(\lambda)$, $\theta^{obs}(\lambda)$) and the parameters of the first

layer ($P_{\max,1}$, $\lambda_{\max,1}$, θ_1). We obtain equations for the polarization degree,

$$P_2(\lambda) = P^{\rm obs}(\lambda)\left(1 - 2r\cos 2\Delta\theta + r^2\right)^{1/2}, \quad (3)$$

and the position angle,

$$\theta_2(\lambda) = \frac{1}{2}\arctan\frac{\sin 2\theta^{\rm obs}(\lambda) - r\sin 2\theta_1}{\cos 2\theta^{\rm obs}(\lambda) - r\cos 2\theta_1}, \quad (4)$$

where $r = P_1(\lambda)/P^{\rm obs}(\lambda)$, $\Delta\theta = \theta^{\rm obs}(\lambda) - \theta_1$. A similar approach has been used by, for example, Messinger, Whittet & Roberge (1997).

Furthermore, from P_2, θ_2 derived at different wavelengths, $P_{2,x}(\lambda)$, $P_{2,y}(\lambda)$ should be calculated and these dependences fitted with Serkowski curves. However, a number of factors make it reasonable to assume that the first layer weakly affects the maximum wavelength of the second layer, that is, $\lambda_{\max,2} \approx \lambda_{\max}^{\rm obs}$. First, for most stars we have $P_{\max,2}/P_{\max,1} < 3$. Second, we have $\lambda_{\max,2} \sim 0.7\,\mu$m and hence the first layer mainly affects the polarization observed in the B and V bands, where for reddened stars the uncertainties of $P^{\rm obs}$ are in any case large (see Table 3). Third, the subtraction of the first layer contribution introduces an additional inaccuracy in the results, as to some extent θ_1 (and $P_{\max,1}$) should vary from one star to another.

In order to check the accuracy of the approximation, we have calculated $P^{\rm obs}(\lambda)$ from equation (2) for various values of the parameters ($P_{\max,1}$, $\lambda_{\max,1}$, $P_{\max,2}$, $\lambda_{\max,2}$) in the cases of $\Delta\theta = 0^\circ$ and 90° and fitted the derived dependences with the Serkowski curve. We found that for $P_{\max,1} = 0.75$ per cent, $\lambda_{\max,1} = 0.56\,\mu$m, $P_{\max,2} = 2.0$ per cent, $\lambda_{\max,2} = 0.7\,\mu$m, which are typical of our reddened stars, the relative difference of $\lambda_{\max,2}$ and $\lambda_{\max}^{\rm obs}$ is less than 5 per cent for $\Delta\theta = 0^\circ$ and 10 per cent for $\Delta\theta = 90^\circ$. For other values of $\Delta\theta$, the effect should be of the same order, while the apparent rotation of the position angle with a changing wavelength is too weak in comparison with the observational errors, as can be seen in Section 5.2.4.

We applied our two-layer model with the discussed approximation to the polarization data for six stars (S3–6, S11–12) seen through B5 and for the star S8 seen through the periphery (rather diffuse) region of B5 ($A_{V,2} \sim 1$ mag) and having some extra extinction ($A_V^{\rm obs} \sim 1.6$ mag). As a result, we obtain estimates of $A_{V,2}$ and $P_{\max,2}$, which are presented in Figs 4–6, where for simplicity we use the following notation: A_V, $P_{\max}$ for the observed (initial) values $A_V^{\rm obs}$, $P_{\max}^{\rm obs}$, and A'_V, $P'_{\max}$ for the corrected ones $A_{V,2}$, $P_{\max,2}$, respectively. The application of our model is considered as a correction of the initial values for the foreground material.

5.2.2 *Relationship between* $\lambda_{\max}$ *and* A_V

Fig. 4 presents the dependence of the wavelength of maximum polarization $\lambda_{\max}$ on the extinction inside B5, A'_V, for several stars seen through this globule. We cross-hatch a region of the values typical of the diffuse ISM and note that the parameters obtained by us for dust foreground to B5 (an extension of the Taurus complex) are inside this region. Within it is also the additional (to foreground) extinction and polarization for the star S8.

The six stars (S3–6, S11–12) seen through B5 display the well-known trend – an increase of $\lambda_{\max}$ with A_V (see e.g. Andersson & Potter 2007; Andersson et al. 2015). It is likely that the highest value of $\lambda_{\max}$ for the star S4 is caused by errors; the other objects are in a region occupied by stars seen through dense clouds (see e.g. Andersson & Potter 2007; Whittet et al. 2008).

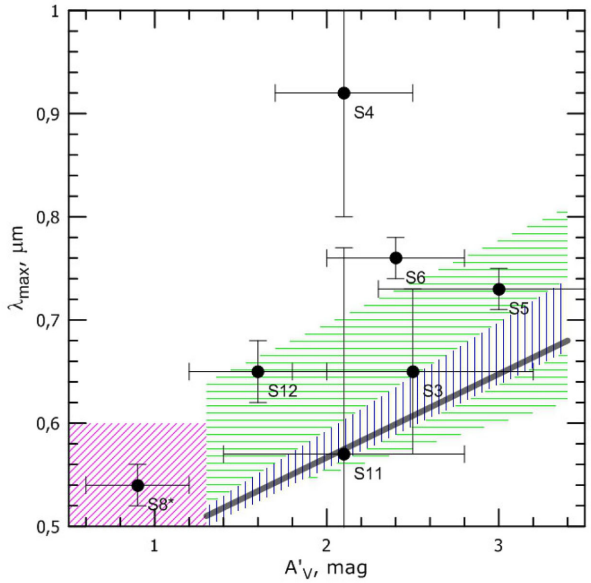

Figure 4. Dependence of the wavelength of maximum polarization $\lambda_{\max}$ on extinction corrected for the foreground, A'_V, for the stars located behind B5. The cross-hatched (magenta) region shows the values typical of the diffuse ISM, the horizontal (green) and vertical (blue) regions indicate the values observed for several molecular clouds (Andersson & Potter 2007) and Taurus field stars (Whittet et al. 2008), respectively, and the thick line presents the mean dependence $\lambda_{\max}(A_V)$ from the latter paper. S8* shows the parameters of dust in the Perseus complex (B5 halo) along the line of sight to the star S8.

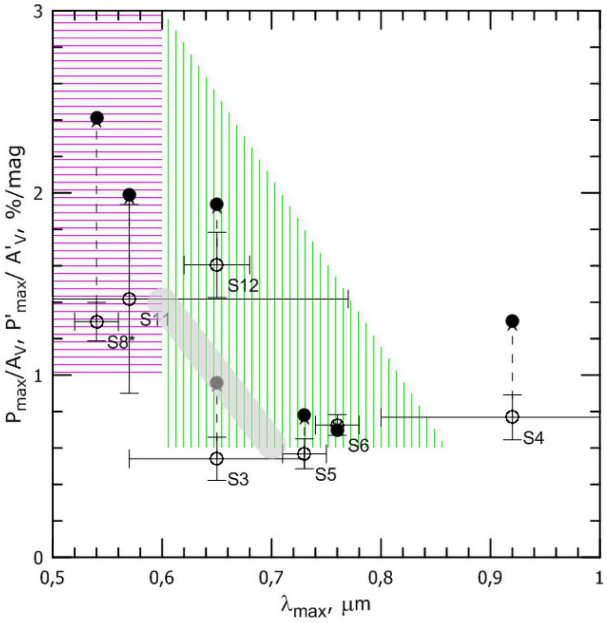

Figure 5. Dependence of the polarizing efficiency on the parameter $\lambda_{\max}$ The uncorrected ($P_{\max}/A_V$) and corrected ($P'_{\max}/A'_V$) values are denoted by open and filled circles, respectively. Horizontal (magenta) hatching indicates values typical of the diffuse ISM; vertical (green) hatching and the broad (gray) band show the position of stars in various molecular clouds (Voshchinnikov & Hirashita 2014) and Taurus field stars (Whittet et al. 2001), respectively.

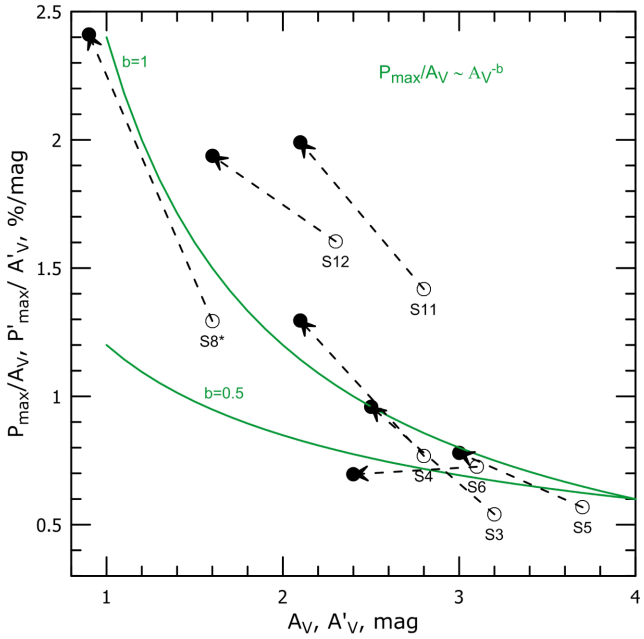

Figure 6. Dependence of the polarizing efficiency on extinction A_V (or A'_V). The initial (P_{max}/A_V) and foreground-corrected (P'_{max}/A'_V) values are given by open and filled circles, respectively. The curves illustrate the often-mentioned theoretical dependences (see the text for more details).

Fitting the data for these six stars with and without S4 gives the trends $\lambda_{max} = 0.506 + 0.088A_V$ and $\lambda_{max} = 0.470 + 0.086A_V$, respectively. The slope (∼0.09) agrees with that found for Taurus field stars by Whittet et al. (2008) and is significantly larger than the slope (equal to 0.01–0.05) found for several star-forming regions by Andersson & Potter (2007). Note that the slope is usually related to variations of the degree of grain alignment with changing depth into a cloud, while the value of $\lambda_{max}(A_V)$ at $A_V = 0$ is then associated with a difference in the grain size distribution in the clouds (for more details see Andersson & Potter 2007). After vertical shifts of the trends $\lambda_{max}(A_V)$ for different clouds by $\Delta\lambda_{max} = \lambda_{max}(A_V = 0) - 0.54 \approx R_V/6 - 0.54$ μm, where $R_V = A_V/E(B-V)$, the extended region of the parameter values becomes much more compact (see e.g. Andersson et al. 2015).

Unfortunately, because of large uncertainties in the APASS B photometry we cannot properly evaluate R_V for our stars: for S3–S6 we obtained $R_V \approx 3.4 \pm 1$, and for S12, $R_V = 2.4 \pm 0.7$ (no B data for S11). Formally, we have $\langle R_V \rangle = 3.3$, which gives a negligible vertical shift $\Delta\lambda_{max} \approx -0.01$ μm, according to the relationship of Andersson et al. (2015), but its uncertainty can be as large as 0.15 μm.

The stars S3–S6 are sufficiently bright (V = 12–14 mag) for good photometry in the B and V bands. If this photometry confirms our value of $\langle R_V \rangle$, then for $A_V \gtrsim 2.2$ mag we would find $\lambda_{max} \gtrsim 0.65$ μm, which would point to a significant increase of the mean grain size occurring before the formation of the ice mantles at $A_V > 3.2 \pm 0.1$ mag (e.g. Boogert, Gerakines & Whittet 2015).

In relation to this, it would be interesting to see in Fig. 4 also several stars seen through the extended ($A_V \sim 1$ mag) B5 halo studied, for example those by Bensch (2006). Unfortunately, there are only two such stars (S8, S9), and, moreover, the star S9 is a variable M giant with a very uncertain estimate of A_V. The position of S8 (its extinction in the B5 halo, $A'_V < 0.9 \pm 0.3$ mag, is comparable to the foreground extinction, $A_{V,1} = 0.7 \pm 0.2$ mag) in Fig. 4 shows that the value of λ_{max} in the halo (and the mean grain size) may not strongly differ from that typical of the diffuse ISM (which generally agrees with $\Delta\lambda_{max} \approx 0$ μm). Therefore, the multicolour polarimetry of stars seen through the halo of B5 is of interest as at the moment it cannot be excluded that large dust grains will occur in the halo too.

Note that the substraction of the foreground extinction ($\Delta A_V = A_V - A'_V = 0.7$ mag) weakly affects the slope of the trend $\lambda_{max}(A_V)$, but shifts it horizontally, which is in our case equivalent to a vertical shift $\Delta\lambda_{max} \approx 0.7 \times 0.09 \approx 0.06$ μm, which is significant. So, accounting for the foreground extinction (and the background one if possible in other cases) can be important for a correct joint consideration of the trend in different clouds.

Finally, we can formulate the main result given by our data — for the extinction in B5 $A'_V > 2$ mag, we found $\lambda_{max} \approx 0.7$ μm, which differs considerably from the $\lambda_{max} = 0.52 - 0.58$ μm derived by us for the diffuse medium in the direction of B5. It should be added that Wang et al. (2017) have recently measured polarization of about 2000 stars background to the filamentary cloud IC 5146 in the R_c, i', H, K bands. They found that the grain properties changed significantly at $A_V \sim 3$ mag, and $\lambda_{max} \approx 0.6$–$0.9$ μm already for $A_V > 2.5$ mag. Their results agree well with our conclusion for globule B5.

5.2.3 *Correlation of* P_{max}/A_V *with* λ_{max} *and* A_V

Another important parameter of a dusty medium is its polarizing efficiency P_{max}/A_V. Fig. 5 presents the dependence of this parameter on λ_{max} for the stars seen through B5. We also show a region of the parameter values obtained for a large set of stars observed though the diffuse ISM and some molecular clouds (for more details see Voshchinnikov et al. 2016).

The correction of the parameters for the effect of foreground is shown by arrows. Note that this correction always decreases the extinction; however, it can increase the polarization degree, as follows from equation (3), provided that $\Delta\theta_0 < \Delta\theta < 2\pi - \Delta\theta_0$, where $\Delta\theta_0 = \arccos(r/2)/2$, and decrease it otherwise. As a result, the correction can slightly decrease the parameter P_{max}/A_V (as in the case of the star S6) or increase it significantly (as for all other stars) – this increase can be as large as 100 per cent (the case of S3). This may be of some importance for comparisons with the theoretical results. In our case, the correction brings our results into better agreement (except for the questionable star S4) with the data collected by Whittet et al. (2001) and later by Voshchinnikov et al. (2016), namely the stars S3, S5, S6 move to the region typical of dense clouds, and the star S12 seen rather through the B5 halo has a higher value of P_{max}/A_V typical of diffuse ISM (see for example, S8, S11).

An analysis of the relationship between P_{max}/A_V and λ_{max} has recently been performed by Voshchinnikov et al. (2016). They found that both quantities are determined mainly by two parameters: the threshold on the size of aligned silicate grains and the time of grain processing in a cloud. Obviously, more observations are required to apply such an analysis or even more detailed models (see e.g. Siebenmorgen et al. 2017) to the data on B5.

A systematic decline of the polarizing efficiency with optical depth in dense molecular clouds is a well-known observational fact (see e.g. Whittet et al. 2008). This trend is interesting from a theoretical point of view and is considered in Fig. 6.

It can be seen that the correction for the foreground moves the stars to the left, top, namely nearly along the trend usually presented as $P_{max}/A_V \propto A_V^{-b}$ with $b \gtrsim 0.5$ (Andersson et al. 2015). Therefore, the correction affects the trend rather weakly.

Our points better agree with the case of $b \gtrsim 1$, in contrast, for example, to the results of Whittet et al. (2001), who found a trend with $b \approx 0.7$ for the field stars behind the Taurus complex. Obviously, our estimate of b requires confirmation from more accurate and extensive observations.

5.2.4 *Wavelength dependence of the position angle*

The two-layer model predicts that such a dependence will be better seen when the polarization maximum wavelengths in the layers $\lambda_{max,\,1}$ and $\lambda_{max,\,2}$ differ significantly, the polarization degrees $P_{max,\,1}$ and $P_{max,\,2}$ are comparable, and the position angle difference $\Delta\theta = \theta_2 - \theta_1$ deviates from 0°and 90°. For the stars seen through B5, these conditions are fulfilled to only a small extent, and a strong wavelength dependence of the position angle should not be expected. However, as the observational data show some position angle variations, it is worthwhile to compare them with the predictions of the model used.

We adopt the polarization characteristics of the foreground layer from Section 5.1 and the parameters $P_{max,2} \equiv P'_{max}$ and θ_2 derived by applying our model to the stars (S3–S6, S12). The star S11 is excluded as its polarization position angle was accurately measured at only two wavelengths. Using equations (2), we calculate the model dependences $\theta(\lambda)$ and compare them with the observational data obtained in this and other works in Fig. 7, in which a couple of erroneous values are not shown as they are outside the plots.

Obviously, the data are too noisy (in particular in the B and V bands) for a reliable comparison of the theory with observations. At first glance, we can merely conclude that the observational data generally do not contradict the predictions of the two-layer model.

Although the linear approximation of the dependence $\theta(\lambda)$ can be applied only in a limited range of wavelengths, we use it in a wider region to make the comparison slightly more quantitative. For stars S3, S4, S5 and S6, we obtained the slope $|(d\theta/d\lambda)_{obs}| = 5$–$6.5$ deg μm^{-1}, while our model gives $|(d\theta/d\lambda)_{calc}| = 2.5$–$8.5$ deg μm^{-1} (for S12, the model predicts $\theta(\lambda) \approx$ const). Bearing in mind the large uncertainties of the data, this agreement seems satisfactory.

We note that a consideration of $\theta(\lambda)$ can become really constraining, provided that the accuracy of polarization measurements in the B band can be made as small as $\delta P < 0.1$ per cent (giving $\delta\theta \sim 1°$), which does not look impossible for the stars S4, S5 and S6 with $V = 12$–14 mag.

6 CONCLUSIONS

We made *UBVRI* polarimetric observations of 10 stars in the B5 region, some of which are seen through the outer layers of this globule with an optical thickness of $\tau_V \sim 3$, and significantly improved the estimates of the polarization parameters λ_{max} and P_{max}. Recent surveys (*Gaia*, LAMOST, APASS, etc.) enabled us to estimate the distance and visual extinction to the stars observed.

Using data from the literature, we also found the distance and visual extinction to 29 additional stars around B5. The information on these stars and the stars observed enabled us to estimate the parameters of the extinction and polarization arising in the Taurus complex, which is foreground to B5: $A_V = 0.7 \pm 0.2$ mag, $P_{max} = 0.75 \pm 0.25$ per cent, $\theta = 50° \pm 20°$ and $\lambda_{max} = 0.56 \pm 0.03$ μm.

We applied a two-layer model with the parameters of the first (foreground) layer given above (the second layer is B5 and its halo) to the data for several stars behind B5 and evaluated the contribution of the globule to the measured extinction and polarization. We considered the effects of such a correcting approach (including the changes of the position angle with wavelength) and noted that it should be applied to many other stars polarimetrically observed through the Perseus cloud complex before a comparison with the theory is made.

We also discussed the relationship between the extinction (A_V) and polarization (P_{max}, λ_{max}) formed in the outer layers of B5 and noted that after our correction they became more similar to those typical of larger molecular clouds. We found a good correlation

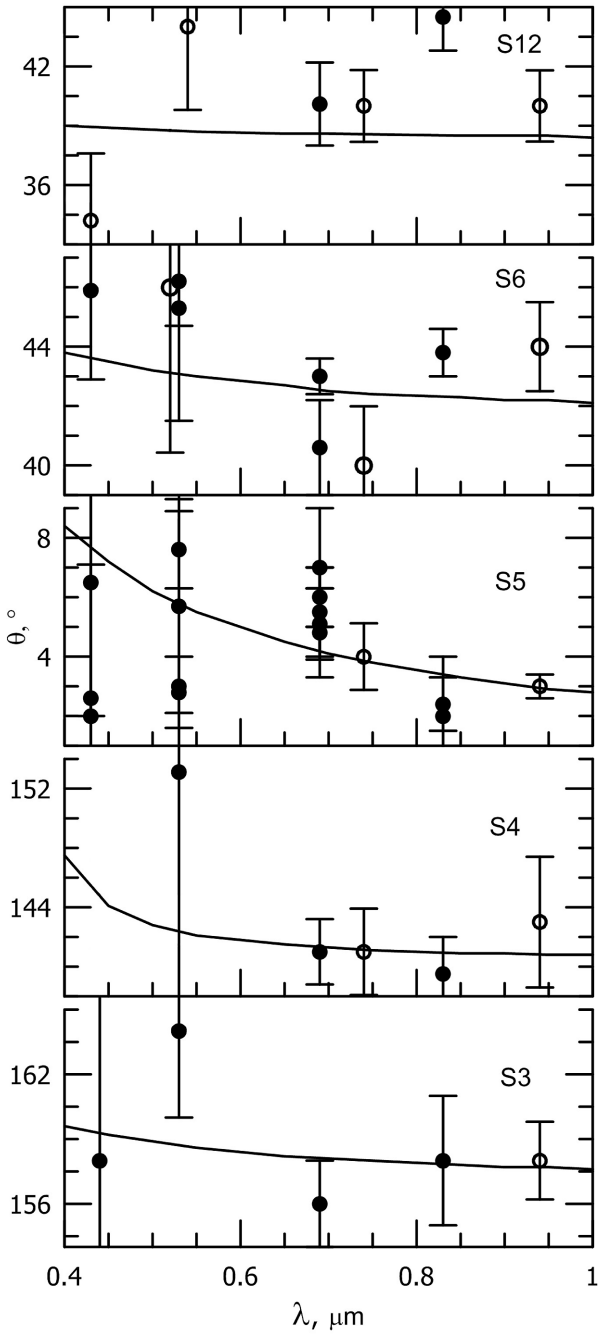

Figure 7. Dependence of the position angle θ on the wavelength λ for stars S3, S4, S5, S6 and S12 located behind B5. The filled and open circles present the observational data obtained in this and other works, respectively. The curves show the predictions of the two-layer model used.

between the position of the observed stars in 3D extinction maps, the extinction to them and their value of λ_{max}. It is worth noting that for the stars seen through the globule layers with $A_V = 2$–3 mag, we derived $\lambda_{max} = 0.6$–0.8 μm, which differs significantly from the value of $\lambda_{max} = 0.52$–0.58 μm obtained by us for the diffuse ISM towards B5. This difference indicates that the dust in the very outer parts of this globule has very specific properties and is in agreement with results reported for other molecular clouds.

ACKNOWLEDGEMENTS

The authors wish to express their gratitude to their friend N.V. Voshchinnikov, who suddenly passed away on December 17th, 2017, for many helpful comments.

This work was partly supported by RFBR grant 16-02-00194, RFBR-DST grant 16-52-45005 and a grant from the St Petersburg University of Aerospace Instrumentation.

This research has made use of the SIMBAD data base and data from the ESA mission *Gaia* and the following surveys and catalogues: LAMOST DR2, APASS DR9, TASS Mark IV, Tycho 2, 2MASS, UCAC4 and others.

The SIMBAD data base is operated at CDS, Strasbourg, France (Wenger, Ochsenbein & Egret 2000). Data from the European Space Agency (ESA) mission *Gaia* (https://www.cosmos.esa.int/gaia) were processed by the *Gaia* Data Processing and Analysis Consortium (DPAC, https://www.cosmos.esa.int/web/gaia/dpac/consortium). Funding for the DPAC is provided by national institutions, in particular the institutions participating in the *Gaia* Multilateral Agreement. Guoshoujing Telescope (the Large Sky Area Multi-Object Fiber Spectroscopic Telescope, LAMOST) is a National Major Scientific Project built by the Chinese Academy of Sciences. Funding for the project was provided by the National Development and Reform Commission. LAMOST is operated and managed by the National Astronomical Observatories, Chinese Academy of Sciences. The AAVSO Photometric All-Sky Survey (APASS) was funded by the Robert Martin Ayers Sciences Fund. The Two Micron All Sky Survey is a joint project of the University of Massachusetts and the Infrared Processing and Analysis Center/California Institute of Technology, funded by the National Aeronautics and Space Administration and the National Science Foundation.

REFERENCES

Andersson B.-G., Potter S. B., 2007, ApJ, 665, 369
Andersson B.-G., Wannier P. G., 1997, ApJ, 491, L103
Andersson B.-G., Lazarian A., Vaillancourt J. E., 2015, ARA&A, 53, 501
Appenzeller I., 1966, Z. Astrophys., 64, 269
Bally J., Walawender J., Johnstone D., Kirk H., Goodman A., 2008, in Reipurt B., ed., Handbook of Star Forming Regions, Vol. 1. Astron. Soc. Pac., San Francisco, p. 308
Belikov A. N., Kharchenko N. V., Piskunov A. E., Schilbach E., Scholz R.-D., 2002, A&A, 387, 117
Bensch F., 2006, A&A, 448, 1043
Bhatt H. C., 1986, MNRAS, 222, 383
Boogert A. C. A., Gerakines P. A., Whittet D. C. B., 2015, ARA&A, 53, 541
Cardelli J. A., Clayton G. C., Mathis J. S., 1989, ApJ, 345, 245
Chen B.-Q. et al., 2014, MNRAS, 443, 1192
Chen M. C.-Y. et al., 2016, ApJ, 826, 95
Clayton G. C., Martin P. G., 1981, AJ, 86, 1518
Cottaar M. et al., 2015, ApJ, 807, 27
Coyne G. V., Gehrels T., 1967, AJ, 72, 887
Coyne G. V., Wickramasinghe N. C., 1969, AJ, 74, 1179
Coyne G. V., Gehrels T., Serkowski K., 1974, AJ, 79, 565
Černis K., 1987, Ap&SS, 133, 355
Černis K., 1990, Ap&SS, 166, 315
Černis K., 1993, Balt. Astron., 2, 214
Černis K., Straižys V., 2003, Balt. Astron., 12, 301
Damineli A., Almeida L. A., Blum R. D., Damineli D. S. C., Navarete F., Rubinho M. S., Teodoro M., 2016, MNRAS, 463, 2653
de Zeeuw P. T., Hoogerwerf R., de Bruijne J. H. J., 1999, AJ, 117, 354
Droege T. F., Richmond M. W., Sallman M., 2006, PASP, 118, 1666
Elias J. H., 1978, ApJ, 224, 453
Elyajouri M., Monreal-Ibero A., Remy Q., Lallement R., 2016, ApJS, 225, 19
Fanciullo L., Guillet V., Boulanger F., Jones A. P., 2017, A&A, 602, A7
Foster J. B., Mandel K. S., Pineda J. E., Covey K. R., Arce H. G., Goodman A. A., 2013, MNRAS, 428, 1606
Fuller G. A., Myers P. C., Welch W. J., Goldsmith P. F., Langer W. D., Campbell B. G., Guilloteau S., Wilson R. W., 1991, ApJ, 376, 135
Gaia collaboration, 2016, A&A, 595, A1
Gehrels T., 1974, in Gehrels T., ed., Planets, Stars and Nebulae Studied with Photopolarimetry. Univ. Arizona Press, Tucson, p. 168
Goodman A. A., Bastien P., Menard F., Myers P. C., 1990, ApJ 359, 363
Green G. M. et al., 2015, ApJ, 810, 25
Heiles C., 2000, AJ 119, 923
Henden A. A., Templeton M., Terrell D., Smith T. C., Levine S., Welch D., 2016, VizieR On-line Data Catalog: II/336
Herbst W., 2008, in Reipurt B., ed., Handbook of Star Forming Regions, Vol. 1. Astron. Soc. Pac., San Francisco, p. 372
Hirota T. et al., 2008, PASJ, 60, 37
Hog E. et al., 2000, A&A, 355, L27
Huovelin J., Linnaluoto S., Tuominen I., Virtanen H., 1989, A&AS, 78, 129
Il'in V. B., Khudyakova T. N., Reshetnikov V. P., 1994, Astron. Rep., 38, 214
Jetsu L. et al., 1990, A&AS, 85, 813
Johnson H. L., 1966, ARA&A, 4, 193
Joshi U. C., Kulkarni P. V., Bhatt H. C., Kulshrestha A. K., Deshpande M. R., 1985, MNRAS, 215, 275
Kenyon S. J., Dobrzycka D., Hartman L., 1994, AJ, 108, 1872
Kerhonen T., Piirola V., Reiz A., 1984, ESO Mess., 38, 30
Lada C. J., Lomdardi M., Alves J. F., 2009, ApJ, 703, 52
Lallement R., Vergely J.-L., Valette B., Puspitarini L., Eyer L., Casagrande L., 2014, A&A, 561, A91
Lefèvre C. et al., 2014, A&A, 572, A20
Lim T.-H., Min K.-W., Seon K.-I., 2013, ApJ, 765, 107
Loinard L., 2013, in de Grijs R., ed., Proc. IAU Symp. No. 289, Advancing the Physics of Cosmic Distances. Kluwer, Dordrecht, p. 36
Lombardi M., Alves J., 2001, A&A, 377, 1023
Loren R. B., 1976, ApJ, 209, 466
Luo A.-L. et al., 2016, VizieR On-line Data Catalog: V/149
McDonald I., Zijlstra A. A., Watson R. A., 2017, MNRAS, 471, 770
Maheswar G., Lee C. W., Bhatt H. C., Mallik S. V., Dib S., 2010, A&A, 509, A44
Martig M., Fouesneau M., Rix H.-W., 2016, MNRAS, 456, 3655
Martin P. G., 1978, Cosmic Dust. Oxford Univ. Press, Oxford
Messinger D. W., Whittet D. C. B., Roberge W. G., 1997, ApJ, 487, 314
Naoi T. et al., 2006, ApJ, 640, 373
Neckel T., Klare G., Sarcander M., 1980, Inform. Bull. CDS, 19, 61
Nesterov V. V., Kuzmin A. V., Ashimbaeva N. T., Volchkov A. A., Röser S., Bastian U., 1995, A&AS, 110, 367
Ochsenbein F., 1980, Inform. Bull. CDS, 19, 74
Piirola V., 1975, Ann. Acad. Sci. Fenn., Ser. A, VI, Phys., 418
Pineda J. E. et al., 2015, Nature, 518, 213
Planck collaboration XIX, 2015, A&A 576, A104
Press W. H., Teukolsky S. A., Vetterling W. T., Flannery B. P., 2007, Numerical Recipes, 3rd edn: The Art of Scientific Computing. Cambrige Univ. Press, Cambridge
Ridge N. A. et al., 2006, AJ, 131, 2921

Ripepi V., Palla F., Marconi M., Bernabei S., Arellano Ferro A., Terranegra L., Alcalá J. M., 2002, A&A, 391, 587
Schlafly E. F. et al., 2014, ApJ, 786, 29
Scholz R. D. et al., 1999, A&AS, 137, 305
Sen A. K., Mukai T., Gupta R., Das H. S., 2005, MNRAS, 361, 177
Serkowski K., Gehrels T., Wisniewski W., 1969, AJ, 74, 85
Shakhovskoy N. M., Efimov Yu. S., 1972, Izv. Krim. Astrofiz. Obs., 45, 90
Shakhovskoy N. M., Efimov Yu. S., 1976, Izv. Krim. Astrofiz. Obs., 54, 99
Siebenmorgen R., Voshchinnikov N. V., Bagnulo S., Cox N. L. J., 2017, Planet. Sp. Sci., 149, 64
Skrutskie M. F. et al., 2006, AJ, 131, 1163
Steinacker J., Pagani L., Bacmann A., Guieu S., 2010, A&A, 511, A9
Stepnik B. et al., 2003, A&A, 398, 551
Straižys V., 1992, Multicolor Stellar Photometry. Pachart Publ. House, Tucson
Straižys V., Lazauskaite R., 2009, Balt. Astron., 18, 19
Straižys V., Černis K., Bartašūite S., 2001, AJ, 131, 1163
Taquet V., Wirström E., Charnley S. B., Faure A., López-Sepulcre A., Persson C. M., 2017, A&A, 607, A20
Togi A., Witt A. N., St. John D., 2017, A&A, 605, A99
Turnshek D., Turnshek D. E., Craine E. R., 1980, AJ, 85, 1638
Valtaoja L. et al., 1972, AJ, 102, 1946
Voshchinnikov N. V., 2004, Ap. Sp. Phys., 12, 1
Voshchinnikov N. V., Hirashita H., 2014, MNRAS, 445, 301
Voshchinnikov N. V., Il'in V. B., 1987, Sov. Astron. Lett., 13, 157
Voshchinnikov N. V., Il'in V. B., Das H. K., 2016, MNRAS, 462, 2343
Vrba F. J., Ström S. E., Ström K. M., 1976, AJ, 81, 958
Wang S., Juang B. W., 2014, ApJ, 788, L12
Wang J.-W., Lai S.-P., Eswaraiah C., Clemens D. P., Chen W.-P., Pandey A. K., 2017, ApJ, 849, 157
Watson C., Henden A. A., Price A., 2014, VizieR On-line Data Catalog: B/vsx, available at: http://vizier.u-strasbg.fr/viz-bin/VizieR?-source=B%2Fvsx
Wegner W., 2003, Astron. N., 324, 219
Wenger M., Ochsenbein F., Egret D., 2000, A&AS, 143, 9
Whittet D. C. B., Martin P. G., Hough J. H., Rouse M. F., Bailey J. A., Axon D. J., 1992, ApJ, 386, 562
Whittet D. C. B., Gerakines G. A., Hough J. H., Shenoy S. S., 2001, ApJ, 547, 872
Whittet D. C. B., Hough J. H., Lazarian A., Hoang T., 2008, ApJ, 674, 304
Wirström E. S., Charnley S. B., Persson C. M., Buckle J. V., Cordiner M. A., Takakuwa S., 2014, ApJ, 788, L32
Wong Y. H. V., Hirashita H., Li Z.-Y., 2016, PASJ, 68, 67
Ysard N., Köhler M., Jones A., Dartois E., Godard M., Gavilan L., 2016, A&A, 591, A44
Zacharias N., Finch C. T., Girard T. M., 2013, AJ, 145, 44
Zapata L. A., Arce H. G., Brassfield E., Palau A., Patel N., Pineda J. E., 2014, MNRAS, 441, 3696
Zasowski G. et al., 2015, ApJ, 798, 35

APPENDIX A: CLASSIFICATION OF STARS, EXTINCTION AND DISTANCE ESTIMATES

S1: This star is an ecliptic binary with an amplitude of about 0.13 mag in the R band and a period of about 0.7 d (Watson et al. 2014). We took $V = 9.21$ mag at maximum using the values from Tycho 2, TASS, and APASS DR6 included in UCAC4 (Zacharias, Finch & Girard 2013), as DR9 contains an incorrect value, $V = 10.14$ mag.

Spectral data indicate the types A7 (HDE, Nesterov et al. 1995) and F0 (SAO, Ochsenbein 1980), while the Vilnius photometry gives F2V with $d = 132 \pm 30$ pc, $A_V = 0.77 \pm 0.1$ mag and $M_V = 2.9$ mag (Černis 1993).

The proper motion is relatively large (-27.0 ± 0.7, -7.1 ± 0.9 mas yr^{-1} from Zacharias et al. 2013), as is the radial velocity $v_r \approx$ 30–40 km s^{-1} (Cottaar et al. 2015). However, the star is not very close to us as the interstellar polarization degree is $P \approx 0.7$ per cent (Joshi et al. 1985); that is, $A_V > P/3 = 0.24$ mag and on average $A_V \sim 0.5$ mag, which usually means a distance greater than 70–100 pc.

The equivalent width of the diffuse interstellar band observed at 1.527 μm is $E(1.527) = 44 \pm 5$ mA (Elyajouri et al. 2016), which on average corresponds to $A_V \sim 0.44$ mag (Zasowski et al. 2015). An inspection of fig. 11 in Elyajouri et al. (2016) shows that A_V should be in the interval 0.25–0.7 mag, and cannot be larger than 1.1 mag.

The spectral type A7V gives $A_V \sim 1.3$ mag, which disagrees with $E(1.527)$, while the Vilnius photometric type F2 V does not quite agree with observed spectra. So, we assume that the type of this star should be about F0V and then obtain $A_V = 0.9 \pm 0.3$ mag and $d = 125 \pm 20$ pc.

S2: HDE gives F8, while LAMOST DR2 gives $T_{\rm eff} = 6593 \pm 86$ K and $\log g = 4.187 \pm 0.374$, corresponding to F4.5 III–V according to Straižys (1992). The *Gaia* DR1 parallax is 5.06±0.50 mas, the UCAC4 proper motion is 13.4 ± 0.8, -14.6 ± 0.9 mas yr^{-1}, Tycho 2 and TASS give $V = 11.1 \pm 0.1$ mag.

The LAMOST type F4.5 agrees much better with the V, K_s photometry and the parallax values than does F8 from HDE. So, we take the F5 V class, which corresponds to $d = 200$ pc, and obtain $A_V = 1.0 \pm 0.2$ mag.

S3: The 2MASS J, H, K_s data agree best with the type K0 III and $A_V \approx 3.6$ mag. The measured photospheric carbon and nitrogen abundances predict $T_{\rm eff} = 4115$ K and $\log g = 2.0$ (Martig, Fouesneau & Rix 2016), corresponding to the type K4 III, which gives $d \approx 1000$ pc and $A_V \approx 2.5$ mag for the B, V values from APASS and TASS.

Although the proper motion is relatively large (10.1 ± 2.7, -8.1 ± 5.3 mas yr^{-1} from UCAC4), we incline towards the mean case of K2 III, which for available V, K_s magnitudes gives $A_V = 3.2 \pm 0.5$ mag and $d = 660 \pm 200$ pc.

S4: LAMOST DR2 gives $T_{\rm eff} = 4195 \pm 47$ K and $\log g = 1.90 \pm 0.46$, which corresponds to K3.5 III and is in good agreement with the C and N abundance predictions from Martig et al. (2016): $T_{\rm eff} = 4108$ K and $\log g = 1.8$. So, we obtain $d = 1450 \pm 200$ pc and $A_V = 2.8 \pm 0.2$ mag.

S5: The 2MASS J, H, K_s data correspond to type K1 III and $A_V \approx 3.6$ mag. Using $V = 11.68 \pm 0.07$ from APASS DR9, it is possible to refine this to $A_V \approx 3.7$ mag and to estimate $d \approx 315$ pc. However, the accuracy of the JHK_s classification is so low that within 1σ of the JHK_s values is the solution K3 III, $d \approx 480$ pc, $A_V \approx 3.3$ mag. So, we can take approximate values of $d = 315 \pm 150$ pc and $A_V = 3.7 \pm 0.5$ mag.

S6: LAMOST DR2 gives $T_{\rm eff} = 4840 \pm 90$ K and $\log g = 2.5 \pm 0.50$, which corresponds to G9.5 III. Using $V = 13.05 \pm 0.06$ mag (APASS DR9) and $K = 7.93 \pm 0.02$ mag (2MASS), we obtain $d = 690 \pm 100$ pc and $A_V = 3.1 \pm 0.2$ mag.

S7: Černis (1993) gives the type F5 V, with $d = 255 \pm 60$ pc, $A_V = 0.48 \pm 0.1$ mag and $M_V = 3.6$ mag. HDE gives F5, and LAMOST DR2 gives $T_{\rm eff} = 6750 \pm 80$ K and $\log g = 4.12 \pm 0.35$, which corresponds to F3.5 V (Straižys 1992).

The *Gaia* parallax is 3.68 ± 0.31 mas. Using TASS and Tycho 2 photometry ($V = 11.11 \pm 0.04$ mag), for F4 V we obtain $d = 270 \pm 25$ pc and $A_V = 0.5 \pm 0.1$ mag, in very good agreement with Černis (1993).

S8: HDE gives A7, while LAMOST DR2 gives $T_{\rm eff} = 6570 \pm 100$ K and $\log g = 4.0 \pm 0.4$, corresponding to F4.5 III–V.

The *Gaia* parallax is 1.855 ± 0.39 mas; the radial velocity ($v_r = 21 \pm 2\,{\rm km\,s^{-1}}$ from Cottaar et al. 2015) and proper motion (2.8 ± 2, -11.9 ± 0.8 mas yr^{-1} from UCAC4) are relatively large.

If we assume the type F4.5 IV, then, having reliable photometry ($V = 11.26 \pm 0.03$ mag from TASS; $K = 8.72 \pm 0.02$ mag from 2MASS), we derive $A_V = 1.6 \pm 0.1$ mag and $d = 260 \pm 100$ pc. The contradiction with the *Gaia* distance $d = 540 \pm 95$ pc is significant. A better solution could be type F4.5 III, giving $d = 350 \pm 100$ pc and the use of $M_V = 1.0$ mag instead of the mean value for this type $M_V = 2.0$ mag (Straižys 1992). Variations of the spectral type do not lead to a better agreement.

S9: This star is a variable M2 or later-class star with B, V amplitudes of about 0.3–0.4 mag (Il'in et al. 1994) and the TASS index WS $=-4.7$. The 2MASS J, H, K_s data correspond to the type M4 III and $A_V \approx 2.1$ mag. Using the mean $V = 11.1$ mag from Il'in et al. (1994) and $K_s = 3.54 \pm 0.24$ mag from 2MASS, it is possible to derive $A_V = 2.4 \pm 1.2$ mag and $d = 800 \pm 200$ pc. The *JHK* classification is in particular unreliable for this star because of large errors in the J, H, K_s values, and hence the corresponding uncertainty of $(V-K)_0$ does not allow us to accurately estimate A_V. For instance, taking the M5 III class, one obtains $A_V = 1.5$ mag and $d = 900$ pc.

S10: LAMOST DR2 gives $T_{\rm eff} = 5870 \pm 100$ K and $\log g = 3.95 \pm 0.54$, corresponding to F9 III–V. The *Gaia* parallax is 3.03 ± 0.48 mas; the radial velocity ($v_R \approx 28\,{\rm km\,s^{-1}}$ from LAMOST) and the proper motion ($\sim$22 mas yr^{-1} from UCAC4) are large.

Using $V \approx 11.05$ mag from TASS and Tycho2, it is found that the class F9 IV agrees with the *Gaia* parallax. So, we have $A_V = 0.6 \pm 0.25$ mag and $d = 330 \pm 45$ pc.

S11: LAMOST DR2 gives $T_{\rm eff} = 5148 \pm 120$ K and $\log g = 3.61 \pm 0.55$, corresponding to G5 III–IV. As the giant should be at a distance of about 1800 pc, a more probable solution looks to be G5 IV with $A_V = 2.8 \pm 0.5$ mag and $d = 600 \pm 400$ pc. The limits are large because the luminosity class is not very certain (class III cannot be excluded).

S12: LAMOST DR2 gives $T_{\rm eff} = 6426 \pm 215$ K and $\log g = 4.20 \pm 0.45$, corresponding to F5.5 V. The proper motion is relatively large ($\sim 22\,{\rm km\,s^{-1}}$ UCAC4), but the polarization degree $P \sim 3.7$ per cent is large too; that is, the star should be neither too distant, nor too close. With $V = 13.97 \pm 0.14$ mag (APASS DR9) we obtain $A_V = 2.3 \pm 0.2$ mag (in good agreement with *JHK* colours) and $d = 380 \pm 90$ pc.

APPENDIX B: DISTANCE AND INTERSTELLAR EXTINCTION TO THE PERSEUS COMPLEX AND GLOBULE B5

The Perseus molecular cloud complex is part of the Taurus–Perseus–Auriga (TPA) star-formation region that also includes the Perseus OB2 association, the Taurus cloud complex, and the California nebula and molecular cloud, etc. (see fig. 3 d in Lim, Min & Seon 2013). Globule B5 as well as the clouds around the young open cluster IC 348 and the reflection nebula NGC 1333 belong to the Perseus complex described in detail by Bally et al. (2008). The distance to the above-mentioned objects and their position in the TPA region are given in Table B1.

Note that the distance to the NGC 1333 clouds is the most reliable as it was derived from the parallax of a maser measured with VLBI (Hirota et al. 2008). The distance to the IC 348 clouds is less certain: Černis (1993) and Scholz et al. (1999) give 260±65 and 260±25 pc, respectively, while Ripepi et al. (2002) and an analysis of Herbst (2008) suggest 320 and 300±15 pc, respectively. The distance to B5 is deduced mainly from the assumption that the globule is related to the IC 348 clouds and is discussed below in some detail. From Hipparcos data, de Zeeuw et al. (1999) derived the mean distances to the early-type members of the association and to all its members to be equal to 318±27 and 296±17 pc, respectively. The California nebula is excited by ξ Per located at the Hipparcos distance of 380±60 pc. The estimates of the distance to the California molecular cloud are controversial (see the discussion in Lada et al. 2009); for example, the western part of this cloud was studied by Straižys et al. (2001) and found to be at a distance of about 300 pc.

Table B1. Some objects in the Taurus–Perseus–Auriga complex.

Object	TPA part	d [pc]	Ref.
NGC 1333 clouds (PMC)	Western	230–235	(1)
IC 348 clouds (PMC)	Central	300 ± 15	(2)
B5 (PMC)	Central	300, 350	(2,3)
Per OB2 association	Central	300 ± 17	(4,5)
California nebula	Northern	300 ± 75	(6)
California molecular cloud	Northern	∼450	(7)
Taurus cloud complex	Eastern	130–160	(1)

Notes: PMC refers to the Perseus molecular cloud complex.
References for the distances: (1) Loinard (2013); (2) Herbst (2008); (3) Schlafly et al. (2014); (4) de Zeeuw, Hoogerwerf & de Bruijne (1999); (5) Belikov et al. (2002); (6) Straižys, Černis & Bartašiūte (2001); (7) Lada, Lomdardi & Alves (2009).

The mean distance to the Taurus complex is assumed to be 135–140 pc (Elias 1978; Kenyon, Dobrzycka & Hartman 1994), but the clouds are probably spread between 130 and 180 pc (Straižys et al. 2001). The VBLI observations give the distance to several T-Tau stars as about 130 pc (with an error of ∼1 pc) and also show that two such stars are at 147 and 162 pc (Loinard 2013).

Note that the NGC 1333 and IC 348 regions are probably not physically related: in addition to the distance difference of about 70 pc, these regions have a difference of several kilometres per second in the gas velocity (Bally et al. 2008).

The interstellar extinction towards the objects from Table B1 has been studied in several works. The main common conclusion is that there are two layers of dust: the first one at a distance of about 130–160 pc (probably related to an extension of the Taurus complex), and the second one at about 200–300 pc (related to the Perseus complex) (e.g. Straižys et al. 2001). An exception is part of the Per OB2 association, where the second layer seems to be absent (e.g. Straižys et al. 2001; Lim et al. 2013). The two-layer extinction model is also supported by polarimetric and spectral data (Loren 1976; Goodman et al. 1990; Černis & Straižys 2003).

Such a large extension of the Taurus complex (over 25°) was unexpected, as was the fact that the extinction $A_{V,1}$ in the first layer varies weakly across the central part of the TPA region. In particular, Černis (1990) found $\langle A_{V,1}\rangle \approx 0.4$ mag at the distance $d = 160 \pm 20$ pc for NGC 1333; Černis & Straižys (2003) obtained $\langle A_{V,1}\rangle \approx 0.3$ mag at the distance $d \sim 150$ pc for the B1 cloud located close to NGC 1333; Černis (1993) derived $\langle A_{V,1}\rangle \approx 0.7$ mag at the distance $d \sim 160$ pc for IC 348 and $\langle A_{V,1}\rangle \approx 0.95$ mag at the distance $d \sim 170$ pc for Per OB2; and Straižys et al. (2001) found $\langle A_{V,1}\rangle \approx 0.3$ mag at the distance $d \sim 160$ pc for the California nebula. Thus, we can assume that for B5 the foreground extinction in the Taurus complex should be about 0.8 mag.

Further information is provided by special studies and recent surveys of extinction. Using the photometric observations of about 400 stars in the Vilnius system as described by Černis (1987), a 3D distribution of the visual extinction in the TPA region was considered by Černis (1990, 1993); Černis & Straižys (2003). For the eastern part of the Perseus complex, Černis (1993) confirmed the presence of two layers of dust: the first one with $A_V \approx 0.7$–0.9 mag, $d \approx 160$ pc and the second one at $d = 220$–260 pc. The second-layer parameters cannot be adopted for globule B5, as only a few stars close to it (with none seen through B5) were considered. Note that the material more distant than 500 pc could not be studied with this approach.

Various detailed 2D maps of the Perseus complex were obtained within the COMPLETE survey (Ridge et al. 2006). It is well known that the extinction map derived from the 2MASS data using the NICER method (Lombardi & Alves 2001) is a better tracer of the dust density than the extinction maps based on far-IR data because of a warm dust shell around the Perseus complex. A detailed 2D map of the B5 globule was obtained by Foster et al. (2013) from UKIDSS *JHK* data and deep *riz*-photometry made with the 6.5-m MMT. This map indicates that the extinction at the periphery of B5 is about 1.5 mag.

A recent 3D extinction map (Lallement et al. 2014) obtained from Strömgren photometry and Hipparcos parallaxes to some extent agrees with the results of Černis (1993) – the map shows two layers (d = 90–110 and 160–280 pc) that may be physically related. The Galactic Anticentre 3D map (Chen et al. 2014) based on *gri*, 2MASS and WISE photometry indicates some extinction at $d = 400$–800 pc behind IC 348 and NGC 133 (at greater distances there is no significant extinction in this direction). The most recent and detailed 3D extinction map constructed by Green et al. (2015) from 2MASS and Pan-STARR 1 data for 800 million stars shows that extinction towards PMC and B5 occurs mainly at $d < 316$ pc.

The distance to globule B5 needs further discussion. If this globule is physically related to the IC 348 clouds, then we can adopt the estimate of Herbst (2008): $d = 300 \pm 17$ pc. However, several authors have suggested that the Perseus complex may consist of clouds located at different distances that are actually not related (see e.g. Bally et al. 2008).

It is worth noting that, using the Pan-STARR 1 data, Schlafly et al. (2014) have also estimated the distances to many molecular clouds, including one projecting on B5, namely Per $l = 160\overset{\circ}{.}4$, $b = -16\overset{\circ}{.}7$ with $\langle E(B-V)\rangle \approx 1.1$ mag and $d = 352 + 53/-50$ pc. The distance obtained is in even better agreement with the estimate of Herbst (2008) when we note that for several clouds in the NGC 1333 region these authors found a mean distance of $\langle d\rangle = 260$ pc (with a deviation ∼35 pc), while $\langle d\rangle = 230$ pc was expected (see Table B1).

This paper has been typeset from a TEX/LATEX file prepared by the author.